Available online at www.sciencedirect.com

ScienceDirect

journal homepage: www.elsevier.com/locate/issn/15375110

Research Paper

GreenLight – An open source model for greenhouses with supplemental lighting: Evaluation of heat requirements under LED and HPS lamps

David Katzin [a,*], Simon van Mourik [a], Frank Kempkes [b], Eldert J. van Henten [a]

[a] Farm Technology Group, Department of Plant Sciences, Wageningen University, PO Box 16, 6700 AA Wageningen, the Netherlands

[b] Wageningen UR Greenhouse Horticulture, PO Box 644, 6700 AP, Wageningen, the Netherlands

ARTICLE INFO

Article history:
Received 18 December 2019
Received in revised form
9 March 2020
Accepted 11 March 2020

Keywords:
Greenhouse models
Greenhouse lighting
Energy use
LEDs
Crop models
Open source

Greenhouse models are important tools for the analysis and design of greenhouse systems and for offering decision support to growers. While many models are available, relatively few include the influence of supplementary lighting on the greenhouse climate and crop. This study presents GreenLight, a model for greenhouses with supplemental lighting. GreenLight extends state of the art models by describing the qualitative difference between the common lighting system of high-pressure sodium (HPS) lamps, and the newest technology for horticultural lighting - the light-emitting diodes (LEDs). LEDs differ from HPS lamps in that they operate at lower temperatures, emit mostly convective heat and relatively little radiative heat, and can be more efficient in converting electricity to photosynthetically active radiation (PAR). These differences can have major implications on the greenhouse climate and operation, and on the amount of heat that must be supplied from the greenhouse heating system. Model predictions have been evaluated against data collected in greenhouse compartments equipped with HPS and LED lamps. The model predicted the greenhouse's heating needs with an error of 8–51 W m^{-2}, representing 1–12% of the measured values; the RMSE for indoor temperature was 1.74–2.04 °C; and the RMSE for relative humidity was 5.52–8.5%. The model is freely available as open source MATLAB software at https://github.com/davkat1/GreenLight. It is hoped that it may be further evaluated and used by researchers worldwide to analyse the influence of the most recent lighting technologies on greenhouse climate control.

* Corresponding author.
E-mail address: david.katzin1@gmail.com (D. Katzin).

https://doi.org/10.1016/j.biosystemseng.2020.03.010

Nomenclature

State variables

CO_2	Carbon dioxide concentration (mg m^{-3})
T	Temperature (°C)
VP	Vapour pressure (Pa)

Auxiliary states

RH	Relative humidity (%)
CO_2^{ppm}	Carbon dioxide concentration (Ppm)

Flux densities

H	Conductive or convective heat flux density (W m^{-2})
L	Latent heat flux density (W m^{-2})
R	Far infrared radiation (FIR) flux density (W m^{-2})
R_{NIR}	Near infrared radiation (NIR) flux density (W m^{-2})
R_{PAR}	Photosynthetically active radiation (PAR) flux density (W m^{-2})
R_{Glob}	Global radiation flux density (W m^{-2})
$R_{LampAir}$	Short wave (PAR and NIR) radiation flux density from the lamp to the greenhouse air (W m^{-2})
Q	Electric energy flux density (W m^{-2})

External climate inputs

I_{Glob}	Outside global radiation (W m^{-2})
T_{Out}	Outdoor temperature (°C)
T_{Sky}	Sky temperature (°C)
T_{SoOut}	Soil temperature ate outer soil layer (°C)
VP_{Out}	Outdoor vapour pressure (Pa)
v_{wind}	Outdoor wind speed (m s^{-1})

Other symbols

cap	Heat capacity of the associated state (J m^{-2} K^{-1})
heat	Energy input to the greenhouse through the heating system (W m^{-2})
ME	Mean error
RE	Relative error (%)
RMSE	Root mean squared error
RRMSE	Relative root mean squared error (%)
U	Controlled input (greenhouse actuator)

Subscripts

Air	Greenhouse air in the main compartment (below the screens)
BlScr	Blackout screen
Boil	Flux from boiler to the pipe rail heating system
BoilGro	Flux from boiler to the grow pipes heating system
Can	Canopy
Cov	Cover
d	Discharge coefficient
e	External side
Ext	External CO_2 source
Flr	Floor
Gh	Greenhouse
Glob	Global radiation
GroPipe	Grow pipes heating system
HEC	Heat exchange coefficient
IntLamp	Inter-lights
in	Indoor side
Lamp	Greenhouse lamp
Leak, *Leakage*	Leakage ventilation
Out	Outside air
Pipe	Pipe rail heating system
Rf, *Roof*	Greenhouse roof
Sky	Sky
So(j)	The jth soil layer
Sun	The sun
Top	Greenhouse air above the screens
ThScr	Thermal screen
Vent	Ventilation
w	Wind coefficient

Superscripts

mes	Measured value
sim	Simulated value

1. Introduction

Greenhouse climate models are a useful tool for the analysis, design, and optimisation of greenhouse structures and climate control. Such models have been in use for several decades, and are continually being extended and developed (Lopez-Cruz, Fitz-Rodríguez, Salazar-Moreno, Rojano-Aguilar, & Kacira, 2018). One reason that greenhouse models must be constantly redeveloped is because greenhouse systems themselves evolve. Some recent progress in greenhouse design and technology include novel heating systems and sources; advanced approaches in crop management and protection; and the introduction of innovative technologies for assimilation lighting (Ahamed, Guo, & Tanino, 2019; Hemming et al., 2017; Marcelis et al., 2014; Marcelis & Heuvelink, 2019; Stanghellini, van't Ooster, & Heuvelink, 2019).

Assimilation lighting has been used in greenhouses for decades and is a rapidly developing greenhouse technology. In high latitudes, high pressure sodium (HPS) lamps are the main source of assimilation lighting in greenhouses (Marcelis, Costa, & Heuvelink, 2019; Viršilė, Olle, & Duchovskis, 2017), and their efficacy, measured in μmol of photons of photosynthetically active radiation (PAR) per joule of input (μmol J^{-1}), can reach values of around 1.7–1.8 μmol J^{-1} (Nelson & Bugbee, 2014). At the same time, light emitting diodes (LEDs) are gaining interest as a useful source of assimilation lighting in greenhouses (Dutta Gupta, 2017; Mitchell et al., 2015), especially since surpassing HPS lamps in efficacy, and reaching as much as 2.5 μmol J^{-1} (Bugbee, 2017), and even a reported 3 μmol J^{-1} (Horticultural lighting qualified products list, 2020). The efficacy of LEDs is expected to continue to rise, although the current and potential efficacies strongly depend on the spectral output of the lamp (Pattison, Hansen, & Tsao, 2018).

With respect to their influence on the greenhouse climate, LEDs differ from HPS lamps in their output of PAR and near infrared radiation (NIR), their convective heat exchange with the surrounding air and in their operating temperature and emission of far infrared radiation (FIR). In HPS lamps, the conversion rate from electrical input to PAR output is around

35–40%. With LEDs, this value can vary greatly, and ranges from around 30%–70% (De Zwart, Baeza, Van Breugel, Mohammadkhani, & Janssen, 2017; Nelson & Bugbee, 2015). The conversion rate from electrical input to NIR output is 20–22% in HPS lamps, and 0–2% in LEDs (De Zwart, Baeza, Van Breugel, Mohammadkhani, & Janssen, 2017; Nelson & Bugbee, 2015). The majority of heat emitted from LEDs is conductive heat, which must be directed away from the lamp in order to maintain its longevity and efficiency. This is done either by a passive cooling system and heat exchange with the surrounding air, or by an active cooling system which includes electric fans or water pipes (Mitchell et al., 2015). Furthermore, LEDs operate at a considerably lower temperatures than HPS lamps, resulting in lower far infrared radiation (FIR), and providing the possibility of placing LEDs closer to the crop without damaging it. In particular, LEDs offer new opportunities for high-intensity inter-lighting, a technique where lamps are placed between or within the crop rows (Heuvelink, Li, & Dorais, 2018).

At the same time, the heat produced by HPS lamps reduces the demand from the greenhouse heating system (Ahamed et al., 2019). Several experiments have shown that the radiative heat from HPS lamps helps maintain the desired crop temperature, and that greenhouses equipped with LEDs require higher inputs from the heating system (Dieleman et al., 2015; Dueck, Janse, Eveleens, Kempkes, & Marcelis, 2012; Ouzounis, Giday, Kjaer, & Ottosen, 2018). It follows, therefore, that the potential energy savings that are achievable by using LEDs may be offset by the need to provide more energy for heating. Thus, a question that arises is how a greenhouse lighting system influences its heating requirements, and how well do greenhouse climate models predict and describe these requirements under various lighting systems.

Despite the recent advances in horticultural lighting, relatively few greenhouse climate models include the effects of lamps. A recent review listed 30 different greenhouse climate models (Lopez-Cruz et al., 2018). Of these, only two models (De Zwart, 1996; Van Beveren, Bontsema, Van Straten, & Van Henten, 2015) describe the influence of HPS lamps, and none consider LEDs. Since LEDs are qualitatively different from other lighting technologies, including them in an already existing greenhouse model, even one that does include lamps, poses a challenge.

A common approach to include the influence of lamps on greenhouse climate is the assumption that a constant fraction of the electricity supply to the lamps immediately heats the greenhouse air (Ahamed, Guo, & Tanino, 2018; Golzar, Heeren, Hellweg, & Roshandel, 2018; Van Beveren, Bontsema, Van Straten, & Van Henten, 2015a, 2015b). A slightly more sophisticated approach, was used by Altes-Buch, Quoilin, and Lemort (2019) and earlier by De Zwart (1996) to distinguish between the PAR and NIR output of the lamps, but lump together FIR and convective heat. Two recent platforms that describe the qualitative differences between HPS and LED lighting are the Radiation Monitor (De Zwart et al., 2017), which focuses on the use of thermal screens; and the Virtual Greenhouse (previously named Hortisim) (Körner & Holst, 2017), which is part of the Universal Simulator (Holst, 2013, 2019), an open source modelling platform. However, it seems that no experimental results are available which demonstrate how well these models perform under various types of lighting.

From the above, we conclude that there is a lack of accessible and tested models that thoroughly describe the influence of assimilation lights, and in particular LEDs, on the crop, the greenhouse climate, and their interactions. Such a model is necessary for reliably predicting the implications of replacing HPS lamps by LEDs. More specifically, such a model should accurately estimate the energy requirements of the heating system in a greenhouse with HPS or LED lamps. In this way, the model can help growers choose and design a lighting system that best suits their circumstances and purposes, as well as assist policy makers in making informed decisions regarding the influence of lighting on greenhouse energy consumption.

The purpose of this study was to design and evaluate a greenhouse climate model which includes a detailed description of assimilation lights (HPS and LEDs). The ability of the model to accurately predict the heat requirements of illuminated greenhouses was tested by comparing model predictions with data collected from greenhouse compartments with HPS and LED lighting. The model developed, named GreenLight, was based on the work of Vanthoor, Stanghellini, van Henten, and de Visser (2011) and Vanthoor, de Visser, Stanghellini, and van Henten (2011), and was extended by adding top-lights, inter-lights, heating pipes within the canopy ("grow pipes"), and a blackout screen to reduce light pollution from the greenhouse to the outside environment. To facilitate reuse and extension of the model, it is publicly and freely available as open source MATLAB code at https://github.com/davkat1/GreenLight.

2. Materials and methods

2.1. *The GreenLight model*

The GreenLight model is based on the model of Vanthoor and Visser et al. (2011) and Vanthoor and Stanghellini, et al. (2011) (termed here the Vanthoor model). The model considers three attributes of the greenhouse climate: energy balance, carbon balance, and vapour balance. The full details of the Vanthoor model are available in the electronic appendices published in Vanthoor and de Visser et al. (2011) and Vanthoor and Stanghellini, et al. (2011). This model was extended to include lamps above the crop (top-lights), lamps within the canopy (inter-lights), heating pipes within the canopy ("grow pipes"), and a blackout screen, which is used to reduce light pollution from the greenhouse towards the outside environment. This section describes some of the main features of the GreenLight model, namely the energy balance model and the lamp model. The full details of the GreenLight model are presented in Appendix A and in the MATLAB code that accompanies this publication.

2.1.1. *Energy balance*

The Vanthoor model includes 13 state variables describing the temperatures of greenhouse objects (°C). These are the temperatures of: the external side of the cover $T_{Cov,e}$; the internal side of the cover $T_{Cov,in}$; the air in the compartment above the thermal screen T_{Top}; the thermal screen T_{ThScr}; the air in the

main compartment T_{Air}; the canopy T_{Can}; the pipe rail system T_{Pipe}; the floor T_{Flr}; and 5 soil layers T_{So1}, T_{So2}, … T_{So5}. In GreenLight, 4 state variables were added: T_{Lamp}, $T_{IntLamp}$, $T_{GroPipe}$, and T_{BlScr}, expressing the temperature of the top-lights, the inter-lights, the grow pipes, and the blackout screen (°C), respectively.

Accompanying the 4 new state variables are 4 new control inputs: U_{Lamp}, $U_{IntLamp}$, $U_{BoilGro}$, and U_{BlScr} describing, respectively, the switching of the top-lights, the switching of the inter-lights, the valve opening between the boiler and the grow pipes, and the opening of the blackout screen. As in the Vanthoor model, control inputs are expressions varying from 0 to 1, where 0 indicates no action (a switched off lamp, a closed heating valve, an open screen), and 1 indicates action at full capacity (a switched-on lamp, a fully open valve, a fully closed screen). A scheme describing the energy balance of the GreenLight model, highlighting the difference between it and the Vanthoor model, is given in Fig. 1.

The differential equations for the temperature states (all in W m^{-2}) are given below. The equations for the lamp temperatures T_{Lamp} and $T_{IntLamp}$ are given in the next subsection. Expressions in bold are additions to the Vanthoor model.

$$
\begin{aligned}
cap_{Cov,e}\dot{T}_{Cov,e} &= R_{Glob_{SunCov,e}} + H_{Cov,inCov,e} - H_{Cov,eOut} - R_{Cov,eSky}\\
cap_{Cov,in}\dot{T}_{Cov,in} &= H_{TopCov,in} + L_{TopCov,in} + R_{CanCov,in} + R_{FlrCov,in}\\
&\quad + R_{PipeCov,in} + R_{ThScrCov,in} - H_{Cov,inCov,e}\\
&\quad + \mathbf{R_{BlScrCov,In}} + \mathbf{R_{LampCov,in}}\\
cap_{Top}\dot{T}_{Top} &= H_{ThScrTop} + H_{AirTop} - H_{TopCov,in} - H_{TopOut} + \mathbf{H_{BlScrTop}}\\
\mathbf{cap_{BlScr}}\dot{\mathbf{T}}_{\mathbf{BlScr}} &= \mathbf{H_{AirBlScr}} + \mathbf{L_{AirBlScr}} + \mathbf{R_{CanBlScr}} + \mathbf{R_{FlrBlScr}} + \mathbf{R_{PipeBlScr}}\\
&\quad - \mathbf{H_{BlScrTop}} - \mathbf{R_{BlScrCov,in}}\\
&\quad - \mathbf{R_{BlScrSky}} - \mathbf{R_{BlScrThScr}} + \mathbf{R_{LampBlScr}}\\
cap_{ThScr}\dot{T}_{ThScr} &= H_{AirThScr} + L_{AirThScr} + R_{CanThScr} + R_{FlrThScr} + R_{PipeThScr}\\
&\quad - H_{ThScrTop} - R_{ThScrCov,in} - R_{ThScrSky}\\
&\quad + \mathbf{R_{BlScrThScr}} + \mathbf{R_{LampThScr}}\\
cap_{Air}\dot{T}_{Air} &= H_{CanAir} + H_{PipeAir} + R_{Glob\_SunAir} - H_{AirFlr} - H_{AirThScr}\\
&\quad - H_{AirOut} - H_{AirTop} - \mathbf{H_{AirBlScr}} + \mathbf{H_{LampAir}}\\
&\quad + \mathbf{R_{LampAir}} + \mathbf{H_{IntLampAir}} + \mathbf{H_{GroPipeAir}}\\
cap_{Can}\dot{T}_{Can} &= R_{PAR\_SunCan} + R_{NIR\_SunCan} + R_{PipeCan} - H_{CanAir} - L_{CanAir}\\
&\quad - R_{CanCov,in} - R_{CanFlr} - R_{CanSky} - R_{CanThScr} - \mathbf{R_{CanBlScr}}\\
&\quad + \mathbf{R_{PAR\_LampCan}} + \mathbf{R_{NIR\_LampCan}} + \mathbf{R_{FIR\_LampCan}}\\
&\quad + \mathbf{R_{PAR\_IntLampCan}} + \mathbf{R_{NIR\_IntLampCan}} + \mathbf{R_{FIR\_IntLampCan}}\\
&\quad + \mathbf{R_{GroPipeCan}}\\
cap_{Pipe}\dot{T}_{Pipe} &= H_{BoilPipe} - R_{PipeSky} - R_{PipeCov,in} - R_{PipeCan} - R_{PipeFlr}\\
&\quad - R_{PipeThScr} - H_{PipeAir} - \mathbf{R_{PipeBlScr}} + \mathbf{R_{LampPipe}}\\
cap_{Flr}\dot{T}_{Flr} &= H_{AirFlr} + R_{PAR\_SunFlr} + R_{NIR\_SunFlr} + R_{CanFlr} + R_{PipeFlr}\\
&\quad - H_{FlrSo1} - R_{FlrCov,in} - R_{FlrSky} - R_{FlrThScr} - \mathbf{R_{FlrBlScr}}\\
&\quad + \mathbf{R_{PAR\_LampFlr}} + \mathbf{R_{NIR\_LampFlr}} + \mathbf{R_{FIR\_LampFlr}}\\
cap_{So(j)}\dot{T}_{So(j)} &= H_{So(j-1)So(j)} - H_{So(j)So(j+1)}\ \ j = 1, 2, \ldots, 5\\
\mathbf{cap_{GroPipe}}\dot{\mathbf{T}}_{\mathbf{GroPipe}} &= \mathbf{H_{BoilGroPipe}} - \mathbf{R_{GroPipeCan}} - \mathbf{H_{GroPipeAir}} \qquad (1)
\end{aligned}
$$

here, H represents conductive or convective heat exchange (W m^{-2}); R represents radiative heat exchange (W m^{-2}); and L represents latent heat exchange (W m^{-2}). Subscripts represent the source and target of the exchange, thus e.g., $R_{Obj1Obj2}$ represents radiative heat exchange from Obj1 to Obj2. The latent heat exchanges depend on the vapour fluxes in the greenhouse, which are described in full by Vanthoor and Stanghellini, et al. (2011).

The blackout screen was modelled in an analogous way to the Vanthoor model component of the thermal screen, with different parameter values. Here, cap_{BlScr} (J K^{-1} m^{-2}) is the heat capacity of the blackout screen; $R_{CanBlScr}$, $R_{FlrBlScr}$, $R_{PipeBlScr}$, $R_{BlScrCov,in}$, $R_{BlScrSky}$, $R_{BlScrThScr}$ and $R_{LampBlScr}$ (W m^{-2}) are, the long wave (FIR) heat exchanges between the blackout screen and, respectively, the canopy, floor, heating pipes, cover, sky, thermal screen, and lamps; $H_{AirBlScr}$ and $H_{TopBlScr}$ (W m^{-2}) are the convective heat exchange between the air in the main and top compartment and the blackout screen; and $L_{AirBlScr}$ (W m^{-2}) is latent heat exchange between the air and the blackout screen due to vapour condensation.

The grow pipes were modelled analogously to the Vanthoor model component for the pipe rail system. However, since for a mature crop the majority of the radiative heat from the grow pipes is absorbed by the canopy, the FIR exchange between the grow pipes and other greenhouse objects was assumed to be negligible. In the equations above, $cap_{GroPipe}$ (J K^{-1} m^{-2}) is the heat capacity of the grow pipes; $H_{BoilGroPipe}$ (W m^{-2}) is the heating input into the grow pipes; $R_{GroPipeCan}$ (W m^{-2}) is the FIR exchange between the grow pipes and the canopy; and $H_{GroPipeAir}$ (W m^{-2}) is the convective heat exchange between the grow pipes and the air in the main compartment.

2.1.2. The lamp model

The equations for the lamp temperatures T_{Lamp} and $T_{IntLamp}$ are (in W m^{-2}):

$$
\begin{aligned}
cap_{Lamp}\dot{T}_{Lamp} &= Q_{LampIn} - R_{LampSky} - R_{LampCov,In} - R_{LampThScr}\\
&\quad - R_{LampBlScr} - H_{LampAir} - R_{PAR\_LampCan}\\
&\quad - R_{NIR\_LampCan} - R_{FIR\_LampCan} - R_{LampPipe}\\
&\quad - R_{PAR\_LampFlr} - R_{NIR\_LampFlr}\\
&\quad - R_{FIR\_LampFlr} - R_{LampAir} - H_{LampCool}\\
cap_{LampInt}\dot{T}_{LampInt} &= Q_{IntLampIn} - H_{IntLampAir} - R_{PAR\_IntLampCan}\\
&\quad - R_{NIR\_IntLampCan} - R_{FIR\_IntLampCan} \qquad (2)
\end{aligned}
$$

where cap_{Lamp} and $cap_{LampInt}$ are the heat capacities of the top-lights and the inter-lights (J K^{-1}). The energy fluxes (all in W m^{-2}) influencing the top-lights' temperature T_{Lamp} may be divided into the following categories:

- **Electrical input**: Q_{LampIn}.
- **FIR exchange** between the lamps and the sky, cover, thermal screen, blackout screen, canopy, heating pipes, and floor: $R_{LampSky}$, $R_{LampCov,in}$, $R_{LampThScr}$, $R_{LampBlScr}$, $R_{FIR\_LampCan}$, $R_{LampPipe}$, and $R_{FIR\_LampFlr}$.
- **NIR output** towards the canopy and the floor: $R_{NIR\_LampCan}$, $R_{NIR\_LampFlr}$.
- **PAR output** towards the canopy and the floor: $R_{PAR\_LampCan}$, $R_{PAR\_LampFlr}$.
- **Short wave radiation (NIR and PAR)** which is not absorbed by the floor or canopy, assumed to be absorbed by the greenhouse construction elements and transferred to the greenhouse air: $R_{LampAir}$.
- **Convective heat exchange** with the greenhouse air: $H_{LampAir}$.
- **Active cooling**, heat extracted from the lamps and removed from the greenhouse system: $H_{LampCool}$.

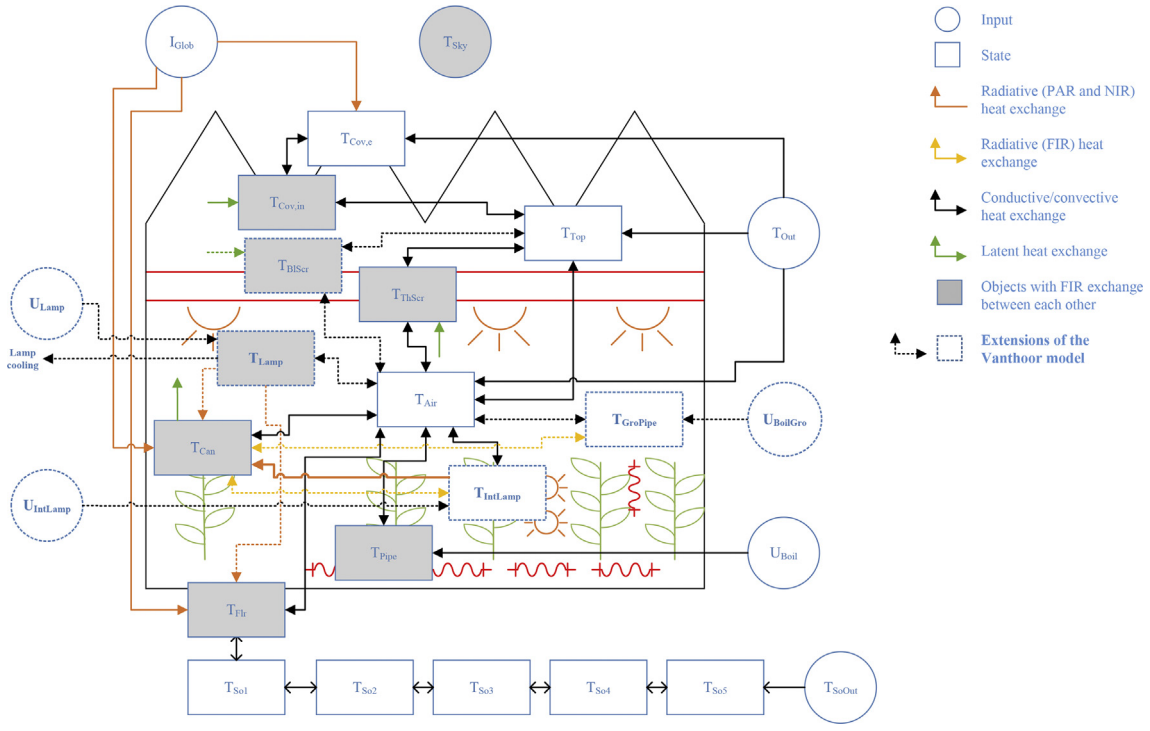

Fig. 1 – Scheme of the GreenLight model energy balance. Dashed and bold items are additions to the Vanthoor model. All the items in grey exchange FIR between each other.

The inter-lights are modelled in a similar way as the top-lights: $Q_{IntLampIn}$ is the electrical input to the interlights; $H_{IntLampAir}$ is the convective heat exchange between the inter-lights and the air; and $R_{PAR\_IntLampCan}$, $R_{NIR\_IntLampCan}$, $R_{FIR\_IntLampCan}$ are, respectively, the PAR, NIR and FIR heat exchanges between the inter-lights and the canopy. As with the grow pipes, radiative heat exchange between the inter-lights and other greenhouse objects was assumed to be negligible.

A total of 15 parameters are used to describe the top-lights: $\theta_{LampMax}$ (W m^{-2}) is the electrical capacity of the lamps; A_{Lamp} (m^2 m^{-2}) is the surface area of the lamps per area of greenhouse floor; $\tau_{LampPAR}$, $\rho_{LampPAR}$, $\tau_{LampNIR}$, $\rho_{LampNIR}$, $\tau_{LampFIR}$ (–) are the transmissivity (τ) and reflectivity (ρ) of PAR, NIR, and FIR of the vertical layer of the lamps. These influence the radiative fluxes in the greenhouse, including the loss of sunlight due to shading by the lamps. $\eta_{LampPAR}$ and $\eta_{LampNIR}$ (J(PAR/NIR) J^{-1}(electricity)) are the conversion rate from electrical input to PAR and NIR output of the lamp; $\zeta_{LampPAR}$ (μmol(PAR) J^{-1}(PAR)) is the amount of photons per joule within the PAR output of the lamps, which depends on the lamps' spectral output; ϵ^{Top}_{Lamp} and ϵ^{Bottom}_{Lamp} (–) are the emissivity of the lamps towards the top and the bottom; $\eta_{LampCool}$ (–) is the amount of energy exported from the lamps by active cooling and removed from the greenhouse, expressed as a fraction of the electrical input; *capLamp* (J K^{-1} m^{-2}) is the heat capacity of the lamps, affecting the rate of heating and cooling of the lamps; and $c_{HEClampAir}$ (W K^{-1} m^{-2}) is the heat exchange coefficient between the lamps and the surrounding air, which influences how much of the energy of a lamp is converted to convective heat, and indirectly, the lamp operating temperature.

The inter-lights require 8 parameters, which are similar to those of the top-lights. These are the electrical capacity of the lamps $\theta_{IntLampMax}$ (W m^{-2}); the surface area of the lamps $A_{IntLamp}$ (m^2 m^{-2}); the conversion rate from electrical input to PAR and NIR output $\eta_{IntLampPAR}$ and $\eta_{IntLampNIR}$ (J(PAR/NIR) J^{-1}(electricity)); the amount of photons per joule within the PAR output of the lamps $\zeta_{LampPAR}$ (μmol(PAR) J^{-1}(PAR)); the emissivity of the lamps $\epsilon_{IntLamp}$ (–); the heat capacity of the lamps *capIntLamp* (J K^{-1} m^{-2}); and the heat exchange coefficient between the lamps and the surrounding air $c_{HEClampAir}$ (W K^{-1} m^{-2}).

The efficacy of the lamps, measured in photons of PAR per joule of electric input, is $\eta_{LampPAR} \cdot \zeta_{LampPAR}$ (μmol(PAR) J^{-1}(electricity)). The maximal photosynthetic photon flux density (PPFD) of the lamp, which is the flow of photons of PAR per m^2 of greenhouse floor area, is $\eta_{LampPAR} \cdot \zeta_{LampPAR} \cdot \theta_{LampMax}$ (μmol(PAR) s^{-1} m^{-2}).

A diagram describing the energy flows to and from the top-lights, as well the main lamp parameters, is presented in Fig. 2. A full description of the lamp model, along with all the modifications made in GreenLight with respect to the Vanthoor model, is given in Appendix A.

2.2. Model evaluation

Data from an experiment comparing HPS and LED top-lights was used for evaluating the GreenLight model. The experiment was described in detail by Dueck et al. (2012, 2010). In this experiment, tomato plants (*Solanum lycopersicum* cv. *Sunstream*) were grown in Bleiswijk, the Netherlands, from 16 October 2009 to 1 July 2010 using a high wire cultivation system. Data from 20 October 2009 to 9 February 2010 (112 days), given in 5-min intervals, was used. The plants were grown in

two neighbouring compartments within an experimental greenhouse, one equipped with HPS top-lights (electric input of 110 W m^{-2}, with an efficacy of 1.8 μmol PAR J^{-1}), and one with LED top-lights (electric input of 116 W m^{-2}, with an efficacy of 1.6 μmol PAR J^{-1}, and an active water cooling system). Both compartments had a pipe rail and grow pipe heating system, thermal and blackout screens. The size of each compartment was 9.6 m by 15 m, with a total floor area of 144 m^2, eave height of 5.7 m and ridge height of 6.7 m. The roof of each compartment consisted of 2 ridges, with a slope of 23°. The compartments were part of a larger greenhouse measuring 120 m by 80 m. Two walls of each compartment faced neighbouring compartments, two walls faced indoor corridors, and the roof faced the outdoor. A scheme of the compartments and their location within the experimental greenhouse is given in Fig. 3.

In each compartment, 12 plant rows were sown, with a plant density and initial stem density of 3.12 plants and stems per m^2. The stem density was increased to 3.9 stems per m^2 on December 14, 2009, and to 4.7 stems per m^2 on January 27, 2010. In the HPS compartment, HPS lamps were hung above two paths, 8 lamps of 1000 W above each path. Lamps were installed at a height of 4.7 m and with a distance of 1.85 m between the lamps.

In the LED compartment, lamps were installed above the crop rows. LEDs from Lemnis Lighting, the Netherlands were used. These lamps were water-cooled to maintain their efficacy, and heat extracted by the cooling system was removed from the greenhouse. The LED lighting was composed of 12% blue LEDs (with a peak at 450 nm) and 88% red LEDs (with a peak at 660 nm). The LEDs were installed at a height of 4.65 m. In both compartments, the light distribution from the lamps was measured during the night using a Sunscan Canopy analysis system (Delta-T Ltd, Cambridge, UK), to ensure a uniform distribution of PAR light from the lamps.

The PPFD from the lamps above the crop was 170 μmol m^{-2} s^{-1} in both compartments. The maximum daylength was 18 h, and the lamps were switched off one hour before sundown. The setting for CO_2 concentration was 1000 ppm. Irrigation, leaf and flower pruning, and temperature set points were modified dynamically by observing the state of the crop with a team of experts with the aim of maximizing production. In the data used for this study, lamps were on for an average of 14 h a day, and the average CO_2 concentration was 1000 ppm in both compartments. In the HPS compartment, the average air temperature for the light and dark period was 21.5 °C and 18.5 °C, respectively. In the

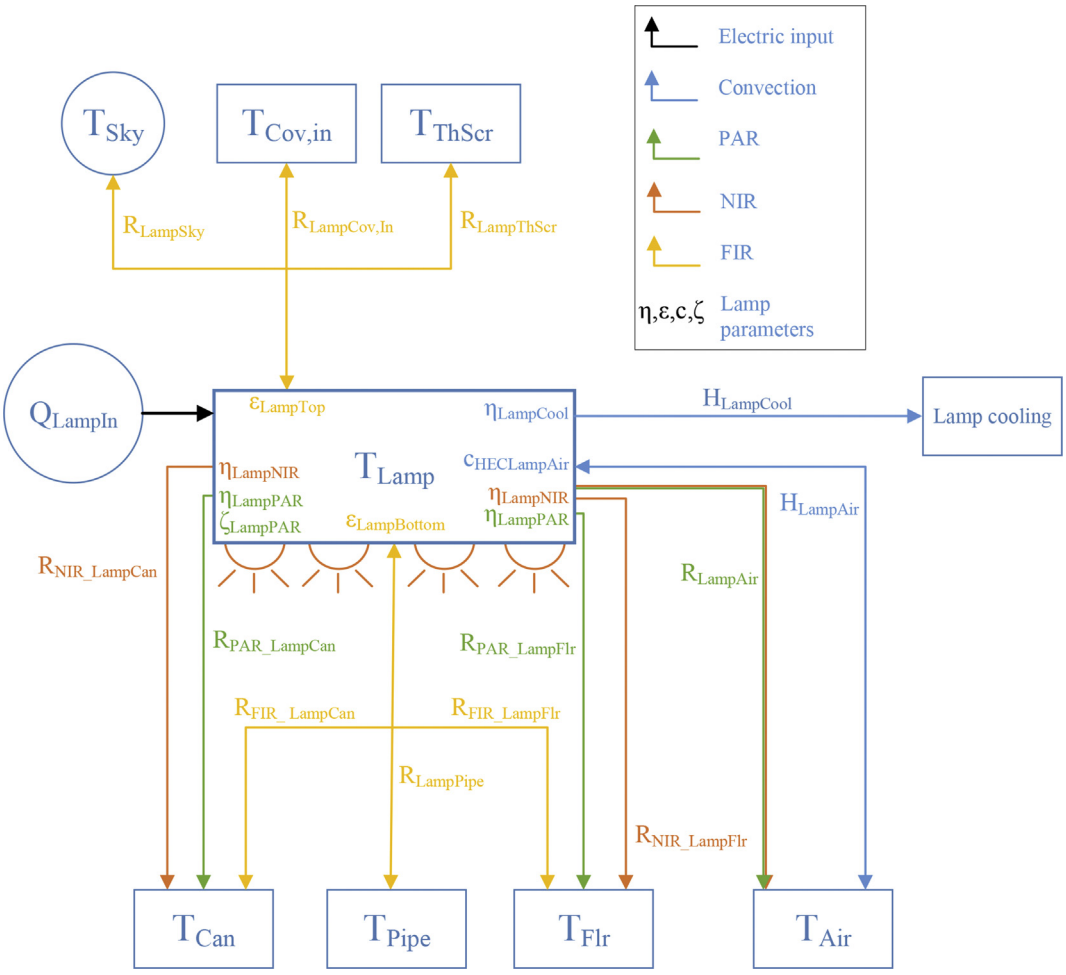

Fig. 2 – The energy flows to and from the lamp, including FIR, NIR, PAR, and convective heat exchange, as well as the main lamp parameters in the GreenLight model. See Appendix A for full details.

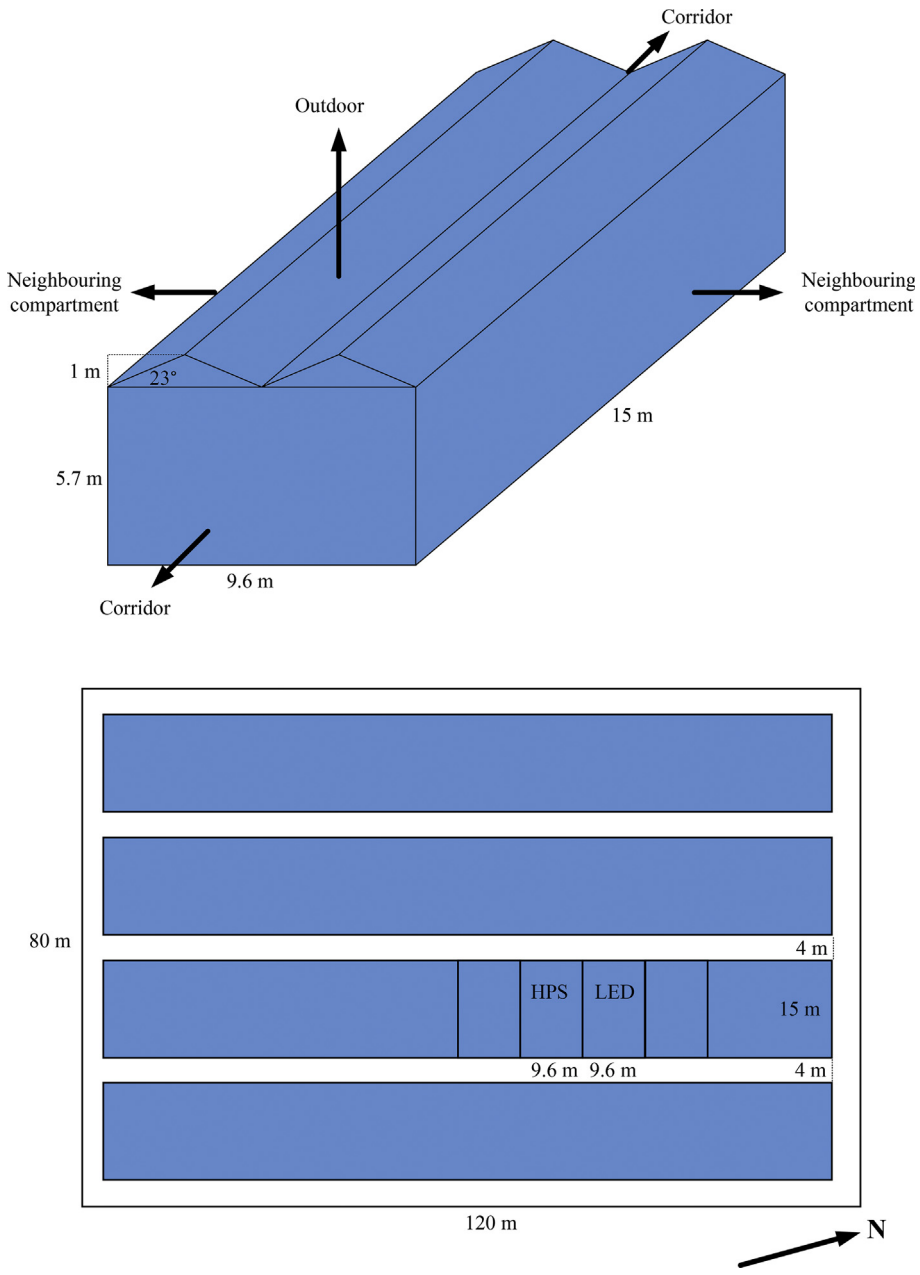

Fig. 3 – Above: 3-D view of an experimental compartment used for collection of data for evaluation of the GreenLight model. Two walls of each compartment faced neighbouring compartments, two walls faced an indoor corridor, and the roof faced the outdoor. Below: location of the compartments with HPS and LED top-lights within the experimental greenhouse. Shaded areas indicate growth compartments, white areas indicate corridors.

LED compartment, the average air temperature for the light and dark period was 22 °C and 19 °C, respectively.

Plants in the HPS compartment were slightly taller than those in the LED compartment throughout the trial. Similarly, the leaf area index (LAI, leaf area per floor area, $m^2\ m^{-2}$), was consistently higher in the HPS compartment, and to a lesser extent, the average number of trusses per stem. A summary of plant growth and development measurements recorded throughout the trial is given in Fig. 4.

The following data, recorded during the trial, was used for model evaluation:

- Outdoor conditions: sun radiation I_{Glob} (W m^{-2}), air temperature T_{Out} (°C), vapour pressure VP_{Out} (Pa), wind speed v_{Wind} (m s^{-1}).
- Indoor conditions: air temperature T_{Air} (°C), relative humidity RH_{Air} (%), CO_2 concentration $CO_{2,Air}^{ppm}$ (ppm).
- Greenhouse actuators: pipe rail temperature T_{Pipe} (°C), grow pipe temperature $T_{GroPipe}$ (°C), window opening U_{Roof} (%), screen closure U_{ThScr}, U_{BlScr} (%), lamp status U_{Lamp} (0–1), CO_2 injection U_{ExtCO_2} (0–1).

Outdoor conditions were measured using a Hoogendoorn weather mast (Hoogendoorn, Vlaardingen, The Netherlands) located on top of the greenhouse service building. Indoor climate was measured by a ventilated Hoogendoorn measurement box, which was placed in the middle of the compartment at the height of the top of the crop. The height of the measurement box was adjusted throughout the experiment to keep it at the top of the crop. All data was collected in 5 min intervals by an Economic Hoogendoorn climate controller.

2.2.1. *Parameter estimation and calibration*

The Vanthoor greenhouse model, and the parameters describing a Dutch greenhouse given in the electronic appendix of Vanthoor and Stanghellini, et al. (2011), were used as a basis for model evaluation. However, several parameters describing the greenhouse structure were modified to describe the compartments used in the current study. Some parameters were taken directly from the greenhouse specifications. These were the mean greenhouse cover slope ψ (°); the floor area of the compartment A_{Flr} (m^2); the height of the main compartment h_{Air} (below the screens, m); the mean height of the greenhouse h_{Gh} (m); maximum roof ventilation area A_{Roof} (m^2); vertical dimension of a single ventilation opening h_{Vent} (m); PAR transmission of the thermal screen $\tau_{ThScrPAR}$ (–) and the blackout screen $\tau_{BlScrPAR}$ (–); PAR and NIR transmission of the roof τ_{Rf}^{PAR}, τ_{Rf}^{NIR} (–); capacity of the CO_2 injection φ_{ExtCo_2} (mg s^{-1}); external and internal diameter of the pipe rail heating $\varphi_{Pipe,E}$, $\varphi_{Pipe,I}$ (m); external and internal diameter of the grow pipes heating $\varphi_{GroPipe,E}$, $\varphi_{GroPipe,I}$ (m); length of the pipe rail heating and the grow pipes heating per floor area l_{Pipe}, $l_{GroPipe}$ (m m^{-2}).

The parameter A_{Cov} (m^2) represents the greenhouse cover area, including the roof and the sidewalls. This parameter influences the heat exchange between the greenhouse and the outdoor air, and assumes that the sidewalls all face the outdoor, which was not the case in this trial. In order to estimate a value for this parameter which correctly expresses the heat exchange between the compartment and the outside air, the area of side walls facing adjacent compartments was neglected, since these compartments had similar temperatures, so it was assumed that heat exchange through these side walls

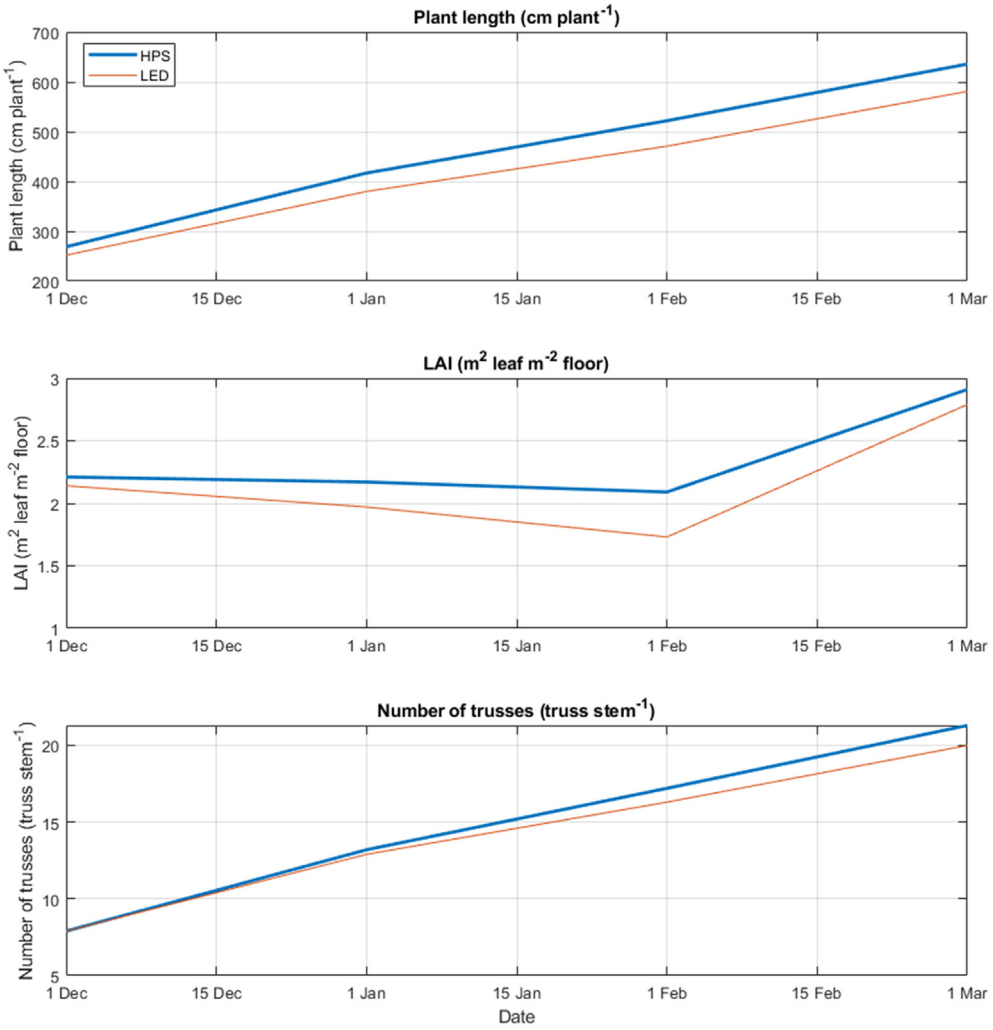

Fig. 4 – Crop growth and development in the HPS and LED compartments throughout the evaluation trial, including average plant length (cm plant^{-1}), leaf area index (LAI, m^2 plant m^{-2} floor), and average number of trusses (truss stem^{-1}).

was negligible. The area of the side walls facing the internal greenhouse corridor (a total of 120 m^2) was multiplied by 0.5, representing the reduced heat loss towards the corridor compared to heat loss to the outside air. The area facing the outside was 156.6 m^2, resulting in $A_{Cov} = 120 \cdot 0.5 + 156.6 = 216.6$ m^2. The value for c_{HECin} (W m^{-2} K^{-1}), which influences the heat exchange between the greenhouse air and the cover material, was set as 3.5 W m^{-2} K^{-1} in order to take into account the large area of the sidewalls in the greenhouse compartments.

Six parameters describe the air flows within the greenhouse and between the greenhouse and the outside: $c_{LeakTop}$ (–) is the fraction of leakage ventilation that originates above the screen; $c_{Leakage}$ (–) influences leakage ventilation, that is, ventilation that is independent of the roof opening; c_d^{Gh} (–) is the ventilation discharge coefficient; c_w^{Gh} (–) is the ventilation global wind pressure coefficient, which influences the effect of wind on ventilation; K_{ThScr} and K_{BlScr} (m^3 m^{-2} $K^{-0.66}$ s^{-1}) are the flux coefficients of the thermal and blackout screen, which influence the effect of screen closure on air flow through the screens.

Since it is difficult to directly measure these parameters, these values were calibrated, based on the recorded data, by considering the indoor CO_2 concentration during the dark periods, thus avoiding the influence of injection and assimilation.

The parameters were fitted, in a stepwise fashion, with the goal of fitting the model predictions of CO_2 concentration in the dark period to the measured values. The value for $c_{LeakTop}$ was assumed to be 0.9, expressing the fact that the majority of leakage ventilation occurred through the roof and not towards the corridor or neighbouring compartments. Next, data from periods when the roof was fully closed and screens were fully open was used to fit $c_{Leakage}$, since in those periods this is the only parameter which influences ventilation rates. Periods with no wind and with fully open screens were then used to calibrate c_d^{Gh}, since in those periods only $c_{Leakage}$ and c_d^{Gh} influence ventilation rates. Periods with fully open screens were used to calibrate c_w^{Gh}, and finally, the entire dark period was used to calibrate K_{ThScr} and K_{BlScr}.

The resulting values for the modified parameters used in the evaluation trial are given in Table 1. These parameters remained constant throughout the simulation.

2.2.2. Estimation of lamp specific parameters

Estimation of the 15 parameters used to describe the toplights (see Section 2.1.2 above) was done as follows: the parameters $\theta_{LampMax}$ and A_{Lamp} were based on direct measurement. For estimating $\tau_{LampPAR}$, $\tau_{LampNIR}$, $\tau_{LampFIR}$, $\rho_{LampPAR}$, $\rho_{LampNIR}$, it was assumed that the lamps fully absorb PAR, NIR and FIR coming from the sun and the objects above, and that reflection is negligible. Since the majority of radiative output of HPS lamps is directed towards the crop, it was assumed that $\varepsilon_{Lamp}^{Bottom}$ was 0.9 and ε_{Lamp}^{Top} was 0.1 for HPS lamps. The emissivity for LEDs was assumed to be 0.88 for both directions, which is equivalent to the emissivity of the heating pipes. This was done based on the observation that LEDs placed within the canopy have a similar heating effect as grow pipes. The conversion rate $\eta_{LampNIR}$ was based on Nelson and Bugbee (2015). The conversion rate $\eta_{LampPAR}$ was also based on Nelson and

Table 1 – Parameters from the Vanthoor model which were modified or added to represent the compartments used in this study. Parameters not given here were set at the default value of the Dutch greenhouse in Vanthoor and Stanghellini, et al. (2011).

Notation	Meaning	Unit	Value
ψ	Mean greenhouse cover slope	°	23
A_{Cov}	Surface area of the cover including side walls facing the outside	m^2	216.6
A_{Flr}	Floor area of the greenhouse	m^2	144
h_{Air}	Height of the main compartment in the greenhouse	m	5.7
h_{Gh}	Mean height of the greenhouse	m	6.2
A_{Roof}	Maximum roof ventilation area	m^2	52.2
h_{Vent}	Vertical dimension of single ventilation opening	m	0.87
$c_{Leakage}$	Leakage coefficient	–	$0.3 \cdot 10^{-4}$
c_d^{Gh}	Ventilation discharge coefficient	–	0.35
c_w^{Gh}	Ventilation global wind pressure coefficient	–	0.02
$c_{LeakTop}$	Fraction of leakage ventilation coming from the top compartment	–	0.9
$\tau_{ThScrPAR}$	PAR transmission coefficient of the thermal screen	–	0.75
$\tau_{BlScrPAR}$	PAR transmission coefficient of the blackout screen	–	0.01
K_{ThScr}	Thermal screen flux coefficient	m^3 m^{-2} $K^{-0.66}$ s^{-1}	$5 \cdot 10^{-4}$
K_{BlScr}	Blackout screen flux coefficient	m^3 m^{-2} $K^{-0.66}$ s^{-1}	$5 \cdot 10^{-4}$
τ_{Rf}^{PAR}	PAR transmission coefficient of the roof	–	0.57
τ_{Rf}^{NIR}	NIR transmission coefficient of the roof	–	0.57
c_{HECin}	Convective heat exchange parameter between cover and outdoor air	W m^{-2} K^{-1}	3.5
φ_{ExtCO_2}	Capacity of the external CO_2 source	mg s^{-1}	720
$\varphi_{Pipe,E}$	External diameter of pipe rail heating pipes	m	$51 \cdot 10^{-3}$
$\varphi_{Pipe,I}$	Internal diameter of pipe rail heating pipes	m	$48.75 \cdot 10^{-3}$
l_{Pipe}	Length of pipe rail heating pipes per floor area	m m^{-2}	1.3375
$\varphi_{GroPipe,E}$	External diameter of grow pipes	m	0.035
$\varphi_{GroPipe,I}$	Internal diameter of grow pipes	m	0.0338
$l_{GroPipe}$	Length of grow pipes heating per floor area	m m^{-2}	1.655

Bugbee (2015) but with a correction for the efficacy of the lamps used.

The fraction for cooling of the LEDs $\eta_{LampCool}$ was set at 63%, based on measurements during the trial. Lastly, cap_{Lamp} influences the rate at which the lamp heats and cools, and $c_{HEClampAir}$ influences the convective heat exchange between the lamp and the surrounding air. These parameters were chosen in such a way that the thermal dynamics of the lamps will behave as typically observed in greenhouses. For HPS lamps, a typical operating temperature of around 150 °C was assumed. It was further assumed that the lamps heat up and cool down within around 1 h. For LEDs, it was assumed that without cooling, the lamps can reach operating temperatures of around 55 °C, and that the lamps take around 30 min to heat up and cool down. With cooling, the lamps are around 1 °C warmer than the air when switched on. Simulations were performed with and without lamp cooling in order to test that the lamps behave as expected.

A summary of the lamp parameters used for the evaluation is given in Table 2.

2.2.3. Evaluation of indoor climate predictions

In order to evaluate how well the model predicts the indoor climate of the greenhouse, the recorded outdoor conditions I^{mes}_{Glob}, T^{mes}_{Out}, VP^{mes}_{Out}, v^{mes}_{wind}; and the recorded greenhouse actuators T^{mes}_{Pipe}, $T^{mes}_{GroPipe}$, U^{mes}_{Roof}, U^{mes}_{ThScr}, U^{mes}_{BlScr}, U^{mes}_{Lamp}, $U^{mes}_{ExtCO_2}$ were used as inputs to the model. The outdoor CO_2 concentration was assumed to be 400 ppm. Simulations were performed using these values, and the simulated T^{sim}_{Air}, RH^{sim}_{Air}, and $CO^{ppm,sim}_{2,Air}$ were compared against the measured values by calculating the mean error (ME), the root mean squared error (RMSE) and the relative root mean squared error (RRMSE). Using these various measures of error allows to compare our model's prediction with that of other models found in the literature, where various measures appear.

The mean error of the predictions was defined as the average difference between the simulated and measured values:

$$ME = \frac{1}{n}\sum_{i=1}^{n}\left(y_i^{mes} - y_i^{sim}\right) \quad (3)$$

where y_i^{mes} is the measured value at time i; y_i^{sim} is the simulated value at time i; and n is the number of measurements. The measured and simulated data were sampled at 5-min intervals. The mean error has the same unit as the measured and simulated values. A positive ME indicates model overestimation, while a negative ME indicates model underestimation.

The root mean squared error was defined as

$$RMSE = \sqrt{\frac{1}{n}\sum_{i=1}^{n}\left(y_i^{mes} - y_i^{sim}\right)^2} \quad (4)$$

The RMSE provides a measure of prediction error, in the same units as the measured variable y^{mes}. An RMSE close to zero indicates good model predictions.

The relative root mean squared error was defined as

$$RRMSE = \frac{100}{\bar{y}^{mes}}\sqrt{\frac{1}{n}\sum_{i=1}^{n}\left(y_i^{mes} - y_i^{sim}\right)^2} \quad (\%) \quad (5)$$

where $\bar{y}^{mes}$ is the average of the measured values. The RRMSE is a unitless measure of prediction error, allowing to compare between measurements of different units. An RRMSE close to 0% indicates good model predictions. Note that for relative humidity, RMSE is given in percent relative to saturated vapour pressure (relative humidity of 100%), and RRMSE is given in percent relative to the mean relative humidity.

To compare measured and simulated values, the units of the variable VP_{Air} (Pa) were converted to relative humidity RH_{Air} (%). Similarly, $CO_{2,Air}$ (mg m^{-3}) was converted to $CO^{ppm}_{2,Air}$ (ppm). These converted units are more commonly used in greenhouse climate control and are thus easier to interpret.

2.2.4. Evaluation of energy use predictions

To evaluate how well the model predicts the amount of energy needed for heating, the recorded outdoor conditions I^{mes}_{Glob}, T^{mes}_{Out},

Table 2 – Lamp specific parameters used in the GreenLight model, with the values used for model evaluation. The PPFD above the crop was 170 μmol(PAR) m^{-2} s^{-1} in both compartments.

Notation	Meaning	Unit	HPS	LED
$\theta_{LampMax}$	Electrical energy input to the lamps	W m^{-2}	110	116
A_{Lamp}	Surface area of the lamps per area of greenhouse floor	m^2 m^{-2}	0.03	0.05
$\tau_{LampPAR}$	Transmissivity of sun's PAR through the top-lights layer	–	0.97	0.95
$\rho_{LampPAR}$	Reflection of sun's PAR through the top-lights layer	–	0	0
$\tau_{LampNIR}$	Transmissivity of sun's NIR through the top-lights layer	–	0.97	0.95
$\rho_{LampNIR}$	Reflection of sun's NIR through the top-lights layer	–	0	0
$\tau_{LampFIR}$	Transmissivity of FIR through the top-lights layer	–	0.97	0.95
$\eta_{LampPAR}$	Fraction of top-lights electrical input converted to PAR	J(PAR) J^{-1}(input)	0.36	0.31
$\eta_{LampNIR}$	Fraction of top-lights electrical input converted to NIR	J(NIR) J^{-1}(input)	0.22	0.02
ϵ^{Top}_{Lamp}	Emissivity of the top side of the top-lights	–	0.1	0.88
ϵ^{Bottom}_{Lamp}	Emissivity of the bottom side of the top-lights	–	0.9	0.88
$\eta_{LampCool}$	Fraction of lamp energy input that is removed by active cooling	–	0	0.63
$capLamp$	Heat capacity of the lamps	J K^{-1} m^{-2}	100	10
$c_{HEClampAir}$	Heat exchange coefficient between the top-lights and surrounding air	W K^{-1} m^{-2}	0.09	2.3
$\zeta_{LampPAR}$	Photons per joule in PAR emitted by the lamp, depending on the spectral output of the lamp	μmol(PAR) J^{-1}(PAR)	5	5.2
$\eta_{LampPAR}\zeta_{LampPAR}$	Efficacy of the lamp in photons of PAR emitted per joule of electric input	μmol J^{-1}(PAR) J^{-1}(input)	1.8	1.6
$\eta_{LampPAR}\zeta_{LampPAR}\theta_{LampMax}$	Photosynthetic photon flux density (PPFD) of the lamps	μmol(PAR) m^{-2} s^{-1}	198	187

VP^{mes}_{Out}, v^{mes}_{wind}; and all the recorded greenhouse actuators besides the pipe temperatures U^{mes}_{Roof}, U^{mes}_{ThScr}, U^{mes}_{BlScr}, U^{mes}_{Lamp}, $U^{mes}_{ExtCO_2}$ were used as inputs to the model. Furthermore, the measured indoor temperature T^{mes}_{Air} was used as a dynamic setpoint for the simulated heating system. Thus, the simulated greenhouse provided the calculated amount of energy into the heating system required to achieve the same temperatures as those recorded in the actual greenhouse. The simulated heating input required for the entire season, $heat^{sim}$ (MJ m^{-2}), which was calculated by integrating the energy input to the pipes $H^{sim}_{BoilPipe}$ and $H^{sim}_{BoilGroPipe}$ (W m^{-2}), was compared against the measurement of heating input given to the real greenhouse $heat^{mes}$. The relative error in estimation was defined as

$$RE\ heating = 100 \cdot \frac{heat^{sim} - heat^{mes}}{heat^{mes}} \cdot \quad (\%) \tag{6}$$

here, an RE value close to 0 indicates good model predictions; a positive value indicates an overestimation; and a negative value indicates an underestimation of the greenhouse heating needs.

2.3. Source code for the model and simulations

The code used to design the GreenLight model and run the simulations in this study is available in MATLAB format (MATLAB R2019b, The MathWorks) in open source code at https://github.com/davkat1/GreenLight. The model was constructed using the DyMoMa framework (Katzin, 2020), an open-source MATLAB framework for dynamic modelling.

3. Results

The root mean squared error (RMSE), relative root mean squared error (RRMSE), and mean error (ME) of the model predictions of indoor climate, as well as the measured and simulated energy used for heating, are given in Table 3. The simulations of T_{Air} and RH_{Air} give a good fit, while the prediction for $CO^{ppm}_{2,Air}$ is poorer. Most importantly, the estimates for heating requirements are very good, giving an especially accurate fit in the LED compartment. The error in heating predictions (7–50 MJ m^{-2}) are very small in comparison to the difference between the heating input between compartments (350 MJ m^{-2}).

Table 3 – Root mean squared error (RMSE), relative root mean squared error (RRMSE) and mean error (ME) between measured and simulated T_{Air}, RH_{Air}, and $CO^{ppm}_{2,Air}$, and measured and simulated heating inputs in the HPS and LED compartments. Note that for relative humidity, RMSE is given in percent relative to saturated vapour pressure (relative humidity of 100%), and RRMSE is given in percent relative to the mean relative humidity.

	HPS	LED
RMSE T_{Air} (°C)	2.04	1.74
RMSE RH_{Air} (%)	8.50	5.52
RMSE $CO^{ppm}_{2,Air}$ (ppm)	347	361
RRMSE T_{Air} (%)	9.77	8.22
RRMSE RH_{Air} (%)	10.5	6.57
RRMSE $CO^{ppm}_{2,Air}$ (%)	34.1	34.7
ME T_{Air} (°C)	−0.09	0.05
ME RH_{Air} (%)	5.84	2.35
ME $CO^{ppm}_{2,Air}$ (ppm)	36.6	−285
Measured heating (MJ m^{-2})	435	785
Simulated heating (MJ m^{-2})	486	778
RE heating (%)	11.6	−0.92

Figure 5 presents the cumulative simulated and measured heating inputs in the HPS and LED compartments. The heating requirements in the LED compartment are predicted very well throughout the tested season. The heating requirement in the HPS compartment is also predicted well throughout the season, but with a slight underestimation over the last month.

Figure 6 presents a 5-day sample (November 26 to December 1, 2010) which is representative of the measured and simulated climate values in the two greenhouse compartments examined in this study. The bottom row of Fig. 6 shows the energy coming from the sun and lamps, to help differentiate between the light and dark periods during these 5 days. As was also seen in Table 3, the indoor temperatures are predicted very well. The relative humidity is overestimated, especially in the HPS compartment during the light period, while the trends of humidity during the night period are estimated well. In both compartments, the CO_2 concentration is predicted well during the dark period: the modelled rate of increase in CO_2 concentration during the dark period, as a result of crop respiration and ventilation, is similar to the measured rates. However, during the light period there is an overestimation of CO_2 in the HPS compartment and an underestimation in the LED compartment, suggesting there is a possible error in the measured rate of CO_2 injection.

Table 4 shows how the energy input into the lamp was divided into various outputs in the simulation. The values for PAR, NIR, and cooling were set by the model parameters as described in Section 2.2.2. The table shows how the rest of the lamp energy outputs, namely the FIR and convective heat output, have been expressed throughout the simulation.

From Tables 3 and 4 we see that the HPS compartment had a total energy input of 1097 MJ m^{-2}, where 435 MJ m^{-2} went to heating and 662 MJ m^{-2} to lighting. The LED compartment had an energy input of 1461 MJ m^{-2}, with 785 MJ m^{-2} supplied to heating, 676 MJ m^{-2} to lighting, and 426 MJ m^{-2} extracted by cooling. The net energy input of the LED compartment was thus 1035 MJ m^{-2}, which is similar to the energy input of the HPS compartment.

Figure 7 shows a timeline of the simulated lamp and air temperatures on the night between 15 and 16 November 2009, which represents a typical day in the simulated season. The HPS lamps reach close to 150 °C within around 30 min, and cools down slightly slower, returning to room temperature approximately one hour after being switched off. The LED lamp, when no cooling is applied, heats and cools rapidly, with a big jump in temperature when switched on, followed by a more gradual heating. Without cooling, the LED lamp is around 30 °C warmer than the surrounding air. When cooling is applied, the LED when on is about 1.5 °C warmer than the surrounding air, and about 0.3 °C colder than the air when off.

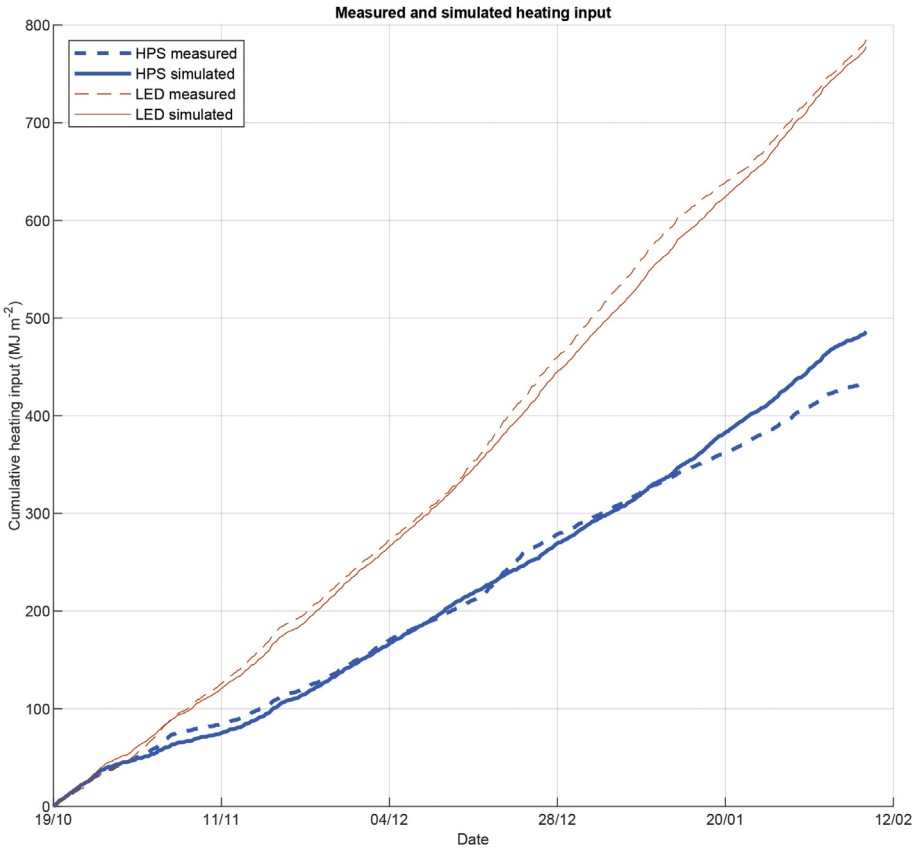

Fig. 5 – Timeline of the measured and simulated heating inputs in the HPS and LED compartments.

4. Discussion

The purpose of this study was to present the GreenLight model and test whether it can be used to predict the energy needed for heating in an illuminated greenhouse. The model closely predicted the heating needs for greenhouse compartments equipped with LEDs and HPS top-lights, as was shown in Fig. 5. The error in model predictions (up to 50 MJ m^{-2}) is considerably smaller than the measured difference in heating requirements between the two lighting systems (350 MJ m^{-2}), demonstrating that the model captures and expresses the differences in heating between the HPS and LED compartment. With regards to the dynamics of the indoor climate predictions, the RMSE of air temperature was around 2 °C, and the RMSE of relative humidity was 5.5–8.5% of saturation. The corresponding RRMSE's were below 10%, except for relative humidity in the HPS compartment which was slightly above 10%. These values are within the range of most greenhouse models, where an RRMSE of 10% or less is considered a good fit (Vanthoor and De Visser, et al., 2011). Other conventions in agricultural modelling consider an RRMSE of less than 10% as excellent (Jamieson, Porter, & Wilson, 1991).

The predictions of indoor climate could be further improved. In particular the model predictions regarding indoor CO_2 concentration could be tested further. The air flows in the model were calibrated based on the measurements of the CO_2 during the dark period, which resulted in a good fit of CO_2 during those times, but the error during the light period was large. A possible cause for the error in CO_2 predictions is a problem with the data regarding the CO_2 injection rates, which was only applied during the light period. Unfortunately, the data available only indicated whether the valve for CO_2 injection was open or not; it was assumed that the injection rate whenever the valve was open φ_{ExtCO_2} was constant and equal to 720 mg s^{-1}. However, the actual injection rate was unfortunately not recorded, and may possibly have varied between compartments and throughout the experiment.

The model also showed a systematic error in simulated relative humidity. Since both the HPS and LED compartments showed an overestimation of humidity, part of this error could be attributed to a misrepresentation of greenhouse structure attributes, such as the rate of condensation on the cover. However, the HPS compartment showed a larger overestimation of humidity, with a mean error of 5.84% in the HPS compartment and 2.35% in the LED compartment. While this error is not large, it could indicate that the model does not yet sufficiently describe the influence of lamp type on crop transpiration. For instance, GreenLight does not take into account the influence of light spectrum on stomatal aperture (Ouzounis, Rosenqvist, & Ottosen, 2015). The model also does not distinguish between the various levels inside the crop canopy. Kim, Lin, and Mitchell (2019) found that while transpiration is considerably higher under HPS in the upper level of the canopy, in lower levels the transpiration rates under HPS and LEDs are similar. Modelling the entire canopy as one

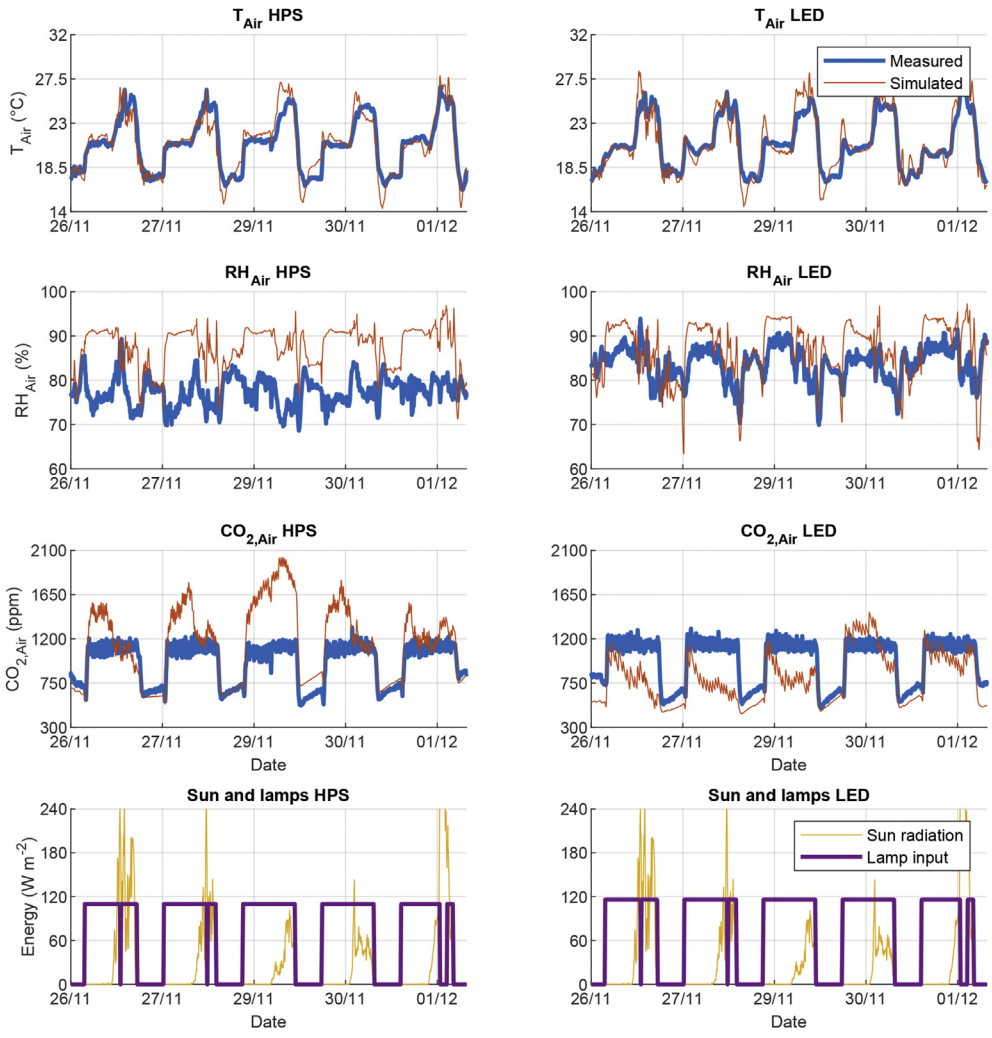

Fig. 6 – Sample of the measured and simulated climate trajectories for T_{Air}, RH_{Air}, and $CO_{2,Air}^{ppm}$ in the HPS and LED compartments. The fourth row presents incoming energy from the sun and lamps, to help indicate the day and night time during the simulations.

Table 4 – Separation of the energy output of each lamp in the simulations performed. Values for PAR, NIR and cooling are a result of the predefined model parameters. Values for FIR and convective output are a result of the simulated model dynamics.

	HPS	LED
Total lamp input (MJ m^{-2})	662	676
PAR output (%)	36	31
NIR output (%)	22	2
FIR output (%)	32.5	2.37
Convective output (%)	9.5	1.63
Cooling (%)	0	63

single surface could thus result in a small overestimation of transpiration under HPS lamps.

The outputs of the GreenLight model quantify the convective and radiative heat emitted by the lamps. The outputs for PAR, NIR and cooling are a result of predefined model parameters, but the output of FIR and convective heat vary in time and depend on the simulated dynamics. In the simulation of the HPS lamp, around 30% of the lamp output was FIR, and around 10% was convective. In the simulation of LEDs, 2% of the output was FIR, with less than 2% released in convection to the air, and 63% as convective cooling. In this study, parameters for PAR and NIR output were based on the measurements of Nelson and Bugbee (2015). The results regarding FIR and convective heat output also agree with those measurements, which indicates that the model's predictions regarding those outputs are also satisfactory.

Nevertheless, the evaluation presented here is based on a single experiment where many parameters had to be estimated and could not be directly measured. Data from more greenhouses, with various lamp settings, could be used to further evaluate and improve the GreenLight model. Regarding lamp specific parameters, Both et al. (2017) suggested a product label for horticultural lamps which, if it becomes standard, would facilitate including new lamps in the GreenLight model, by providing values for many of the parameters used in the model.

One strength of the GreenLight model is that it is available as free an open source code, allowing it to be used by

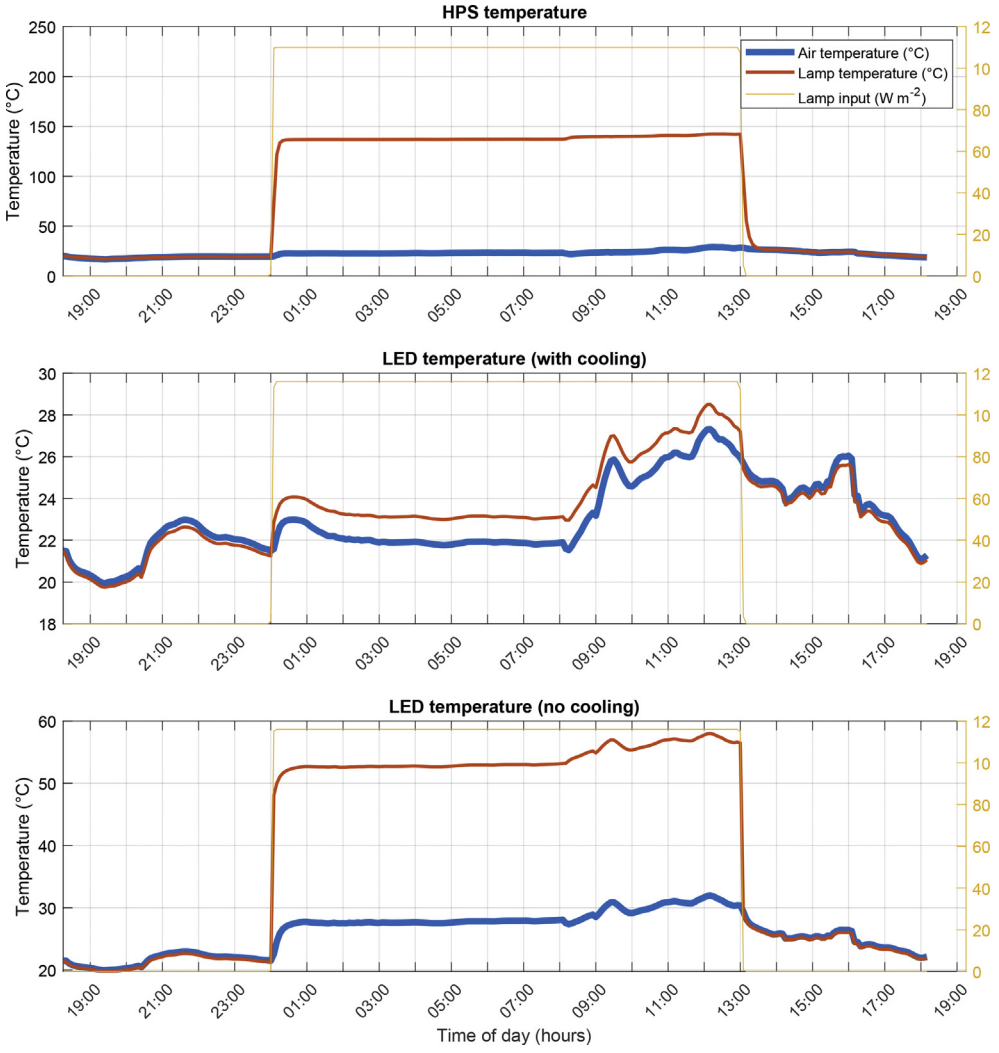

Fig. 7 – Timeline of the simulated lamp and air temperatures on the night between 15 and 16 November 2009. Note the varying scales in the y-axes.

researchers world-wide, to evaluate against their own data and to adapt and further improve the model based on local practice. GreenLight is based on the Vanthoor model which was created to assist in greenhouse design and has been validated for various climate conditions and greenhouse types. In the same way, GreenLight may be used to predict the influence of different lamp types and lighting strategies in various greenhouse types and climates. It would also be beneficial to conduct a sensitivity analysis of the GreenLight model, to test how uncertainties regarding the model parameters and inputs influence predictions.

As can be seen in Fig. 5, during the experiment the heat demand in the LED compartment was almost double that of the HPS compartment: 785 vs 435 MJ m^{-2}. The main reason for the high heating demand in the LED compartment was the active cooling of the LEDs, which extracted 426 MJ m^{-2} of heat from the greenhouse. The net energy input in both compartment was similar. Thus, if a system were installed where the energy extracted by cooling could have been brought back to heat the greenhouse, it is quite possible that the heat demands of the two compartments would have been similar.

At the same time, it should be noted that the experiment considered LEDs that had a similar efficacy to the HPS lamps. Using more efficient LEDs would have resulted in lower electric inputs, which would probably require compensation in the form of higher heating inputs. However, this trade-off between lighting and heating inputs strongly depends on the specific attributes of the lamps, as well as the design of the greenhouse, the dynamics of the indoor climate, the climate control strategy, and the outdoor weather. The GreenLight model provides an important step in developing tools to analyse the influence of these features on illuminated greenhouses.

Declaration of Competing Interest

None declared.

Acknowledgements

The authors would like to thank the editor and anonymous reviewers for helpful remarks that greatly improved this paper. We would also like to thank Anja Dieleman, Bert van 't Ooster, Arie de Gelder, and Feije de Zwart for advice and help in acquisition and analysis of the data used in this study. Further thanks to Mitch Meulensteen for proofreading the manuscript.

Funding for this study was provided as part of the "LED it be 50%" Perspectief programme, supported by the Netherlands Organisation for Scientific Research Domain Applied and Engineering Sciences (NWO-AES), LTO GlaskrachtNederland, Signify, B-Mex, and Ridder Growing Solutions. The funding bodies had no role or influence in the design and conduct of the study; collection, management, analysis, and interpretation of the data; preparation, review, or approval of the manuscript; and decision to submit the manuscript for publication.

Appendix. A. Detailed description of the GreenLight model

As mentioned, the GreenLight model is based on the Vanthoor greenhouse model (Vanthoor and De Visser, et al., 2011; Vanthoor and Stanghellini, et al., 2011). In this section, all the modification made in GreenLight with respect to the Vanthoor model are described. For the Vanthoor model description, see the electronic appendices of Vanthoor and De Visser, et al. (2011) and Vanthoor and Stanghellini, et al. (2011). The GreenLight model and its complete description are available as open source MATLAB code at https://github.com/davkat1/GreenLight.

As mentioned above, the Vanthoor greenhouse model includes 13 state variables describing the temperatures of greenhouse objects (°C). These are the temperatures of: the external side of the cover $T_{Cov,e}$; the internal side of the cover $T_{Cov,in}$; the air in the compartment above the thermal screen T_{Top}; the thermal screen T_{ThScr}; the air in the main compartment T_{Air}; the canopy T_{Can}; the pipe rail system T_{Pipe}; the floor T_{Flr}; and 5 soil layers T_{So1}, T_{So2}, … T_{So5}. In GreenLight, 4 state variables were added: T_{Lamp}, $T_{IntLamp}$, $T_{GroPipe}$, and T_{BlScr}, expressing the temperature of the top-lights, the inter-lights, the grow pipes, and the blackout screen, respectively (°C).

Accompanying the four 4 new state variables are 4 new control inputs: U_{Lamp}, $U_{IntLamp}$, $U_{BoilGro}$, and U_{BlScr} describing, respectively, the switching of the toplights, the switching of the interlights, the valve opening between the boiler and the grow pipes, and the opening of the blackout screen. As in the Vanthoor model, control inputs are unitless expressions varying from 0 to 1, where 0 indicates no action (a switched-off lamp, a closed heating valve, an open screen), and 1 indicates action at full capacity (a switched-on lamp, a fully open valve, a fully closed screen). A scheme describing the energy balance of the GreenLight model, highlighting the difference between it and the Vanthoor model, is given in Fig. 1.

The differential equations for the temperature states (all in W m^{-2}) are given below. Expressions in bold are additions to the Vanthoor model. Greenhouse elements that exist in the Vanthoor model, but were not included here, have been omitted.

$$
\begin{aligned}
cap_{Cov,e}\dot{T}_{Cov,e} &= R_{Glob\_SunCov} + H_{Cov,inCov,e} - H_{Cov,eOut} - R_{Cov,eSky}\\
cap_{Cov,in}\dot{T}_{Cov,in} &= H_{TopCov,in} + L_{TopCov,in} + R_{CanCov,in} + R_{FlrCov,in}\\
&+R_{PipeCov,in} + R_{ThScrCov,in} - H_{Cov,inCov,e} + \mathbf{R_{BlScrCov,In}}+\mathbf{R_{LampCov,in}}\\
cap_{Top}\dot{T}_{Top} &= H_{ThScrTop} + H_{AirTop} - H_{TopCov,in} - H_{TopOut} + \mathbf{H_{BlScrTop}}\\
\mathbf{cap_{BlScr}}\dot{\mathbf{T}}_{\mathbf{BlScr}} &= \mathbf{H_{AirBlScr}} + \mathbf{L_{AirBlScr}} + \mathbf{R_{CanBlScr}} + \mathbf{R_{FlrBlScr}} + \mathbf{R_{PipeBlScr}}\\
&\quad - \mathbf{H_{BlScrTop}} - \mathbf{R_{BlScrCov,in}}\\
&\quad - \mathbf{R_{BlScrSky}} - \mathbf{R_{BlScrThScr}} + \mathbf{R_{LampBlScr}}\\
cap_{ThScr}\dot{T}_{ThScr} &= H_{AirThScr} + L_{AirThScr} + R_{CanThScr} + R_{FlrThScr} + R_{PipeThScr}\\
&\quad - H_{ThScrTop} - R_{ThScrCov,in}\\
&\quad - R_{ThScrSky} + \mathbf{R_{BlScrThScr}} + \mathbf{R_{LampThScr}}\\
cap_{Air}\dot{T}_{Air} &= H_{CanAir} + H_{PipeAir} + R_{Glob\_SunAir} - H_{AirFlr} - H_{AirThScr}\\
&\quad - H_{AirOut} - H_{AirTop} - \mathbf{H_{AirBlScr}} + \mathbf{H_{LampAir}} + \mathbf{R_{LampAir}}\\
&\quad + \mathbf{H_{IntLampAir}} + \mathbf{H_{GroPipeAir}}\\
cap_{Can}\dot{T}_{Can} &= R_{PAR\_SunCan} + R_{NIR\_SunCan} + R_{PipeCan} - H_{CanAir} - L_{CanAir}\\
&\quad - R_{CanCov,in} - R_{CanFlr} - R_{CanSky} - R_{CanThScr} + \mathbf{R_{PAR\_LampCan}}\\
&\quad + \mathbf{R_{NIR\_LampCan}} + \mathbf{R_{FIR\_LampCan}} + \mathbf{R_{PAR\_IntLampCan}}\\
&\quad + \mathbf{R_{NIR\_IntLampCan}} + \mathbf{R_{FIR\_IntLampCan}} + \mathbf{R_{GroPipeCan}}\\
cap_{Pipe}\dot{T}_{Pipe} &= H_{BoilPipe} - R_{PipeSky} - R_{PipeCov,in} - R_{PipeCan} - R_{PipeFlr}\\
&\quad - R_{PipeThScr} - H_{PipeAir} - \mathbf{R_{PipeBlScr}} + \mathbf{R_{LampPipe}}\\
cap_{Flr}\dot{T}_{Flr} &= H_{AirFlr} + R_{PAR\_SunFlr} + R_{NIR\_SunFlr} + R_{CanFlr} + R_{PipeFlr}\\
&\quad - H_{FlrSo1} - R_{FlrCov,in} - R_{FlrSky} - R_{FlrThScr} - \mathbf{R_{FlrBlScr}}\\
&\quad + \mathbf{R_{PAR\_LampFlr}} + \mathbf{R_{NIR\_LampFlr}} + \mathbf{R_{FIR\_LampFlr}}\\
cap_{So(j)}\dot{T}_{So(j)} &= H_{So(j-1)So(j)} - H_{So(j)So(j+1)}\ j = 1, 2, \ldots, 5\\
\mathbf{cap_{GroPipe}}\dot{\mathbf{T}}_{\mathbf{GroPipe}} &= \mathbf{H_{BoilGroPipe}} - \mathbf{R_{GroPipeCan}} - \mathbf{H_{GroPipeAir}}\\
\mathbf{cap_{Lamp}}\dot{\mathbf{T}}_{\mathbf{Lamp}} &= \mathbf{Q_{LampIn}} - \mathbf{R_{LampSky}} - \mathbf{R_{LampCov,In}} - \mathbf{R_{LampThScr}}\\
&\quad - \mathbf{R_{LampBlScr}} - \mathbf{H_{LampAir}} - \mathbf{R_{PAR\_LampCan}} - \mathbf{R_{NIR\_LampCan}}\\
&\quad - \mathbf{R_{FIR\_LampCan}} - \mathbf{R_{LampPipe}} - \mathbf{R_{PAR\_LampFlr}} - \mathbf{R_{NIR\_LampFlr}}\\
&\quad - \mathbf{R_{FIR\_LampFlr}} - \mathbf{R_{LampAir}} - \mathbf{H_{LampCool}}\\
\mathbf{cap_{LampInt}}\dot{\mathbf{T}}_{\mathbf{LampInt}} &= \mathbf{Q_{IntLampIn}} - \mathbf{H_{IntLampAir}} - \mathbf{R_{PAR\_IntLampCan}}\\
&\quad - \mathbf{R_{NIR\_IntLampCan}} - \mathbf{R_{FIR\_IntLampCan}} \qquad \text{(A1)}
\end{aligned}
$$

here, H represents conductive or convective heat exchange (W m^{-2}); R represents radiative heat exchange (W m^{-2}); and L represents latent heat exchange (W m^{-2}). Subscripts represent the source and target of the exchange, thus e.g., $R_{Obj1Obj2}$ represents radiative heat exchange from Obj1 to Obj2. The latent heat exchanges depend on the vapour fluxes in the greenhouse, which are described in full by Vanthoor and Stanghellini, et al. (2011).

The blackout screen was modelled in an analogous way to the Vanthoor model component of the thermal screen, with different parameter values (see Section A.5). Here, cap_{BlScr} (J K^{-1} m^{-2}) is the heat capacity of the blackout screen; $R_{CanBlScr}$, $R_{FlrBlScr}$, $R_{PipeBlScr}$, $R_{BlScrCov,in}$, $R_{BlScrSky}$, $R_{BlScrThScr}$ and $R_{LampBlScr}$ (W m^{-2}) are, respectively, the long wave (FIR) heat exchanges between the blackout screen and the canopy, floor, heating pipes, cover, sky, thermal screen, and lamps; $H_{AirBlScr}$ and $H_{TopBlScr}$ (W m^{-2}) are the convective heat exchange between the air in the main and top compartment and the blackout

screen; and $L_{AirBlScr}$ (W m^{-2}) is latent heat exchange between the air and the blackout screen due to vapour condensation.

The grow pipes were modelled analogously to the Vanthoor model component of the pipe rail system. However, since for a mature crop the majority of the radiative heat from the grow pipes is absorbed by the canopy, the FIR exchange between the grow pipes and other greenhouse objects was assumed to be negligible. In the equations above, $cap_{GroPipe}$ (J K^{-1} m^{-2}) is the heat capacity of the grow pipes; $H_{BoilGroPipe}$ (W m^{-2}) is the heating input into the grow pipes; $R_{GroPipeCan}$ (W m^{-2}) is the FIR exchange between the grow pipes and the canopy; and $H_{GroPipeAir}$ (W m^{-2}) is the convective heat exchange between the grow pipes and the air in the main compartment.

The lamp component of the GreenLight model is used to quantify the PAR, NIR, FIR, and convective outputs of the lamp, in W m^{-2}. The heat capacity of the top-lights (J K^{-1} m^{-2}) is denoted cap_{Lamp}. The electrical input to the top-lights is given by Q_{LampIn}. The PAR output of the top-lights is either absorbed by the canopy ($R_{PAR\_LampCan}$) or by the floor ($R_{PAR\_LampFlr}$). The NIR output of the top-lights is similarly absorbed by the canopy and floor ($R_{NIR\_LampCan}$, $R_{NIR\_LampFlr}$). Long wave radiation (FIR) occurs between the top-lights and the sky, cover, thermal screen, blackout screen, canopy, heating pipes, and floor ($R_{LampSky}$, $R_{LampCov,in}$, $R_{LampThScr}$, $R_{LampBlScr}$ $R_{FIR\_LampCan}$, $R_{LampPipe}$, and $R_{FIR\_LampFlr}$). The convective heat exchange between the top-lights and the surrounding air is given by $H_{LampAir}$, and $R_{LampAir}$ expresses short wave radiation (sum of PAR and NIR) emitted by the top-lights and absorbed by the greenhouse structure. Finally, the energy taken away from the lamp by active cooling is denoted $H_{LampCool}$.

The inter-lights are modelled in a similar way as the top-lights, where $cap_{LampInt}$ (J K^{-1} m^{-2}) is the heat capacity of the inter-lights; $Q_{IntLampIn}$ is the electrical input to the interlights; $H_{IntLampAir}$ is the convective heat exchange between the inter-lights and the air; and $R_{PAR\_IntLampCan}$, $R_{NIR\_IntLampCan}$, $R_{FIR\_IntLampCan}$ are, respectively, the PAR, NIR and FIR heat exchanges between the inter-lights and the canopy. Radiative heat exchange between the inter-lights and other greenhouse objects is assumed to be negligible.

A detailed description of the radiative and convective heat transfers is given below.

A.1. Lumped cover layer

In the Vanthoor model, the optical properties of the movable outdoor shading screen, the semi-permanent shading screen, the greenhouse roof, and the thermal screen are lumped to express the optical properties of the greenhouse cover: τ_{CovPAR}, ρ_{CovPAR}, a_{CovPAR}, τ_{CovNIR}, ρ_{CovNIR}, a_{CovNIR} (–), signifying the transmission, reflection, and absorption coefficients of the lumped cover layer to PAR and NIR, respectively. To calculate the optical properties of lumped layers, the following equations were used in the Vanthoor model:

$$\tau_{12}(\tau_1,\tau_2,\rho_1,\rho_2)=\frac{\tau_1\tau_2}{1-\rho_1\rho_2}(-) \tag{A2}$$

$$\rho_{12}(\tau_1,\tau_2,\rho_1,\rho_2)=\rho_1+\frac{\tau_1^2\rho_2}{1-\rho_1\rho_2}\quad(-) \tag{A3}$$

where τ_1,τ_2 (–) are the transmissivities of each layer, ρ_1,ρ_2 (–) are the reflectivities of each layer, and τ_{12},ρ_{12} (–) are the transmissivity and reflectivity of the resulting lumped layer.

However, the equation for ρ_{12} above neglects the fact that the reflectivity of two objects superimposed on one another depends on which of the objects is facing the light. Thus, the equation for ρ_{12} was replaced by:

$$\tau_{12}\left(\tau_1,\tau_2,\rho_1^{Dn},\rho_2^{Up}\right)=\frac{\tau_1\tau_2}{1-\rho_1^{Dn}\rho_2^{Up}}\quad(-) \tag{A4}$$

$$\rho_{12}^{Up}\left(\tau_1,\rho_1^{Up},\rho_1^{Dn},\rho_2^{Up}\right)=\rho_1^{Up}+\frac{(\tau_1)^2\rho_2^{Up}}{1-\rho_1^{Dn}\rho_2^{Up}}\quad(-) \tag{A5}$$

$$\rho_{12}^{Dn}\left(\tau_2,\rho_2^{Up},\rho_2^{Dn},\rho_1^{Dn}\right)=\rho_2^{Dn}+\frac{(\tau_2)^2\rho_1^{Dn}}{1-\rho_1^{Dn}\rho_2^{Up}}\quad(-) \tag{A6}$$

here, ρ_1^{Up} is the reflectivity towards the top of the object lying on top, ρ_1^{Dn} is the reflectivity towards the bottom of the object lying on top. The rest of the expressions are denoted similarly, where ρ_2 represents the reflectivity of the object on the bottom and ρ_{12} represents the reflectivity of the lumped object.

The equations above have been derived by using Fig. A1. In this figure, a ray of radiation coming from above is labelled 1, the full capacity of the ray. As it passes through the top layer, a fraction τ_1 is transmitted and a fraction ρ_1^{Up} is reflected up. The fraction τ_1 reaches the second layer, where a total fraction $\tau_1\tau_2$ is transmitted, and $\tau_1\rho_2^{Up}$ is reflected. We continue to follow this ray and sum the total fraction that has been transmitted through and reflected by the two layers to arrive at:

$$\tau_{12}=\tau_1\tau_2\sum_{n=0}^{\infty}\left(\rho_1^{Dn}\rho_2^{Up}\right)^n=\frac{\tau_1\tau_2}{1-\rho_1^{Dn}\rho_2^{Up}}\quad(-) \tag{A7}$$

$$\rho_{12}^{Up}=\rho_1^{Up}+(\tau_1)^2\rho_2^{Up}\sum_{n=0}^{\infty}\left(\rho_1^{Dn}\rho_2^{Up}\right)^n=\rho_1^{Up}+\frac{(\tau_1)^2\rho_2^{Up}}{1-\rho_1^{Dn}\rho_2^{Up}}\quad(-) \tag{A8}$$

The equation for ρ_{12}^{Dn} is derived analogously to ρ_{12}^{Up}.

In addition to this change in calculation of reflectivity, two new objects were added to the lumped cover layer, namely the blackout screen and the lamps. The optical properties of all layers except the lamps were thus:

$$\tau_{CovBlScrPAR}=\tau_{12}\left(\tilde{\tau}_{CovPAR},1-U_{BlScr}(1-\tau_{BlScrPAR}),\tilde{\rho}_{CovPAR}^{Dn},U_{BlScr}\rho_{BlScrPAR}\right)\quad(-) \tag{A9}$$

$$\rho_{CovBlScrPAR}^{Up}=\rho_{12}^{Up}\left(\tilde{\tau}_{CovPAR},\tilde{\rho}_{CovPAR}^{Up},\tilde{\rho}_{CovPAR}^{Dn},U_{BlScr}\rho_{BlScr}^{PAR}\right)\quad(-) \tag{A10}$$

$$\rho_{CovBlScrPAR}^{Dn}=\rho_{12}^{Dn}\left(1-U_{BlScr}(1-\tau_{BlScrPAR}),U_{BlScr}\rho_{BlScrPAR},U_{BlScr}\rho_{BlScrPAR},\tilde{\rho}_{CovPAR}^{\sim Dn}\right)\quad(-) \tag{A11}$$

where $\tau_{CovBlScrPAR}$, $\rho_{CovBlScrPAR}^{Up}$, $\rho_{CovBlScrPAR}^{Dn}$ (–) are the transmissivity, reflectivity upwards and reflectivity downwards of PAR for all layers except the lamps; U_{BlScr} is the degree of

closure of the blackout screen (0–1); $\tau_{BlScrPAR}$ (–) is the transmissivity of PAR for the closed blackout screen; $\rho_{BlScrPAR}$ (–) is the reflectivity of PAR for the closed blackout screen; and $\tilde{\tau}_{CovPAR}$, $\tilde{\rho}^{Up}_{CovPAR}$, $\tilde{\rho}^{Dn}_{CovPAR}$ (–) are the transmissivity, reflectivity upwards and reflectivity downwards of PAR to the layers considered in the Vanthoor model, i.e., all layers except the blackout screen and lamps.

The optical properties of all layers were:

$$\tau_{CovPAR} = \tau_{12}\left(\tau_{CovBlScrPAR}, \tau_{LampPAR}, \rho^{Dn}_{CovBlScrPAR}, \rho_{LampPAR}\right) \quad (A12)$$

$$\rho^{Up}_{CovPAR} = \rho^{Up}_{12}\left(\tau_{CovBlScrPAR}, \rho^{Up}_{CovBlScrPAR}, \rho^{Dn}_{CovBlScrPAR}, \rho_{LampPAR}\right) \quad (A13)$$

where τ_{CovPAR}, ρ^{Up}_{CovPAR} (–) are the transmissivity and reflectivity of the entire cover for PAR coming from the sun. $\tau_{LampPAR}$ (–) is the transmissivity to PAR of the lamp layer, i.e., the amount of PAR radiation that passes from above the lamps to right below it. $\rho_{LampPAR}$ (–) is the reflectivity to PAR of the lamp layer, i.e., the amount of PAR radiation that reflects from the lamp layer.

The optical properties for NIR were calculated analogously. The new optical properties of the cover, which include the blackout screen and lamps, replaced the optical properties of the cover used in the Vanthoor model. The optical properties of FIR passing through the cover considered only the shading screens and roof and were thus left the same as in the Vanthoor model.

A.2. Shortwave heat exchange

The PAR above the canopy was supplemented by the PAR emitted by the top-lights:

$$R_{PAR\_GhSun} = (1 - \eta_{Glob\_Air})\tau_{CovPAR} \cdot \eta_{GlobPAR} \cdot I_{Glob}\,(W\,m^{-2}) \quad (A14)$$

$$R_{PAR\_GhLamp} = \eta_{LampPAR} \cdot Q_{LampIn}\,(W\,m^{-2}) \quad (A15)$$

where $\eta_{LampPAR}$ (–) is the fraction of lamp electrical input converted to PAR, and Q_{LampIn} (W m^{-2}) is the electrical input to the lamp, defined by:

$$Q_{LampIn} = U_{Lamp} \cdot \theta_{LampMax}\,(W\,m^{-2}) \quad (A16)$$

where U_{Lamp} (0–1) indicates whether the top-lights are switched on (0 if all lamps are off, 1 if all lamps are on), and $\theta_{LampMax}$ (W m^{-2}) is the electrical input for the top-lights when they are fully on.

The PAR from the top-lights absorbed by the canopy was then calculated analogously to the Vanthoor model:

$$R_{PAR\_LampCan\downarrow} = R_{PAR\_GhLamp}(1 - \rho_{CanPAR})\left(1 - e^{-K_{1\_PAR}LAI}\right) \quad (A17)$$

$$R_{PAR\_LampFlrCan\uparrow} = R_{PAR\_GhLamp}\, e^{-K_{1_{PAR}}LAI}\rho_{FlrPAR}(1 - \rho_{CanPAR})\left(1 - e^{-K_{2\_PAR}LAI}\right)(W\,m^{-2}) \quad (A18)$$

$$R_{PAR\_LampCan} = R_{PAR\_LampCan\downarrow} + R_{PAR\_LampFlrCan\uparrow}\,(W\,m^{-2}) \quad (A19)$$

Similarly, the NIR from the top-lights absorbed by the canopy was calculated analogously to the Vanthoor model:

$$R_{NIR\_LampCan} = \eta_{LampNIR}Q_{LampIn}(1 - \rho_{CanNIR})\left(1 - e^{-K_{NIR}LAI}\right)(W\,m^{-2}) \quad (A20)$$

where $\eta_{LampNIR}$ (–) is the fraction of lamp input converted to NIR.

The PAR and NIR from the top-lights absorbed by the floor was calculated by:

$$R_{PAR\_LampFlr} = R_{PAR\_GhLamp}(1 - \rho_{FlrPAR})e^{-K_{1\_PAR}LAI}\,(W\,m^{-2}) \quad (A21)$$

$$R_{NIR\_LampFlr} = \eta_{LampNIR}Q_{LampIn}(1 - \rho_{FlrNIR})e^{-K_{NIR}LAI}\,(W\,m^{-2}) \quad (A22)$$

PAR and NIR energy emitted by the top-lights and not absorbed by the canopy or floor was assumed to be absorbed by the greenhouse construction elements and immediately transferred to the greenhouse air:

$$R_{LampAir} = \left(\eta_{LampPAR} + \eta_{LampNIR}\right)Q_{LampIn} - R_{PAR\_LampCan} - R_{NIR\_LampCan} - R_{PAR\_LampFlr} - R_{NIR\_LampFlr}\,(W\,m^{-2}) \quad (A23)$$

It was assumed that all PAR and NIR from the inter-lights is absorbed by the canopy:

$$R_{PAR\_IntLampCan} = \eta_{IntLampPAR}Q_{IntLampIn}\,(W\,m^{-2}) \quad (A24)$$

$$R_{NIR\_IntLampCan} = \eta_{IntLampNIR}Q_{IntLampIn}\,(W\,m^{-2}) \quad (A25)$$

where $\eta_{IntLampPAR}$ (–) is the fraction of electrical input to the inter-lights converted to PAR; $\eta_{IntLampNIR}$ (–) is the fraction of electrical input to the inter-lights converted to NIR; and $Q_{IntLampIn}$ (W m^{-2}) is the electrical input to the inter-lights, defined by:

$$Q_{IntLampIn} = U_{IntLamp}\theta_{IntLampMax}\,(W\,m^{-2}) \quad (A26)$$

where $U_{IntLamp}$ (0–1) indicates whether the interlights are switched on (0 if all lamps are off, 1 if all lamps are on), and $\theta_{IntLampMax}$ (W m^{-2}) is the electrical input for the inter-lights when they are fully on.

The global radiation absorbed by the canopy R_{Can}, used for calculating transpiration, was the sum of the NIR and PAR absorbed from the sun, the top-lights, and the inter-lights.

A.3. Long wave (FIR) heat exchange

The long wave (FIR) heat exchange between the greenhouse objects was calculated according to the Stefan–Boltzmann law, as was done by Vanthoor and Stanghellini, et al. (2011) based on the model of De Zwart (1996):

$$R_{i,j} = A_i\varepsilon_i\varepsilon_j F_{i,j}\sigma\left((T_i + 273.15)^4 - (T_j + 273.15)^4\right)(W\,m^{-2}) \quad (A27)$$

where A_i (m^2 m^{-2}) is the surface area of object i per area of greenhouse floor; ε_i, ε_j (–) are the emissivities of objects i and j; $F_{i,j}$ is the view factor between the two objects j; and T_i, T_j are the temperatures of the objects (°C). This equation was used

Table A1 – Parameters regarding long wave (FIR) heat exchange. The lamp areas A_{Lamp} and $A_{IntLamp}$ are parameters that depend on the choice of the lamps. The emissivity of the top-lights ε_{Lamp} is different between the top and the bottom side of the lamp. Thus, two emissivity values ε_{Lamp}^{Top}, $\varepsilon_{Lamp}^{Bottom}$ are used, depending on the direction of radiation emitted from the lamp. Expressions marked in bold are additions to the Vanthoor model.

$FIR_{i,j}$	ε_i	A_i (area)	$F_{i,j}$ (view factor)
$R_{CanCov,In}$	ε_{Can}	$1-e^{-K_{FIR}LAI}$	$\tau_{LampFIR}\tau^{U}_{BlScrFIR}\tau^{U}_{ThScrFIR}$
R_{CanSky}	ε_{Can}	$1-e^{-K_{FIR}LAI}$	$\tau_{LampFIR}\tau^{U}_{BlScrFIR}\tau_{CovFIR}\tau^{U}_{ThScrFIR}$
$R_{CanThScr}$	ε_{Can}	$1-e^{-K_{FIR}LAI}$	$\tau_{LampFIR}\tau^{U}_{BlScrFIR}U_{ThScr}$
R_{CanFlr}	ε_{Can}	$1-e^{-K_{FIR}LAI}$	$1-0.49\pi l_{Pipe}\varphi_{Pipe,e}$
$R_{PipeCov,in}$	ε_{Pipe}	$\pi l_{Pipe}\varphi_{Pipe,e}$	$\tau_{LampFIR}\tau^{U}_{BlScrFIR}\tau^{U}_{ThScrFIR}0.49e^{-K_{FIR}LAI}$
$R_{PipeSky}$	ε_{Pipe}	$\pi l_{Pipe}\varphi_{Pipe,e}$	$\tau_{LampFIR}\tau^{U}_{BlScrFIR}\tau_{CovFIR}\tau^{U}_{ThScrFIR}0.49e^{-K_{FIR}LAI}$
$R_{PipeThScr}$	ε_{Pipe}	$\pi l_{Pipe}\varphi_{Pipe,e}$	$\tau_{LampFIR}\tau^{U}_{BlScrFIR}U_{ThScr}0.49e^{-K_{FIR}LAI}$
$R_{PipeFlr}$	ε_{Pipe}	$\pi l_{Pipe}\varphi_{Pipe,e}$	0.49
$R_{PipeCan}$	ε_{Pipe}	$\pi l_{Pipe}\varphi_{Pipe,e}$	$0.49(1-e^{-K_{FIR}LAI})$
$R_{FlrCov,in}$	ε_{Flr}	1	$\tau_{LampFIR}\tau^{U}_{BlScrFIR}\tau^{U}_{ThScrFIR}\ (1-0.49\pi l_{Pipe}\varphi_{Pipe,e})e^{-K_{FIR}LAI}$
R_{FlrSky}	ε_{Flr}	1	$\tau_{LampFIR}\tau^{U}_{BlScrFIR}\tau_{CovFIR}\tau^{U}_{ThScrFIR}\ (1-0.49\pi l_{Pipe}\varphi_{Pipe,e})e^{-K_{FIR}LAI}$
$R_{FlrThScr}$	ε_{Flr}	1	$\tau_{LampFIR}\tau^{U}_{BlScrFIR}U_{ThScr}\ (1-0.49\pi l_{Pipe}\varphi_{Pipe,e})e^{-K_{FIR}LAI}$
$R_{ThScrCov,in}$	ε_{ThScr}	1	U_{ThScr}
$R_{ThScrSky}$	ε_{ThScr}	1	$\tau_{CovFIR}U_{ThScr}$
$R_{Cov,eSky}$	ε_{Cov}	1	1
$R_{LampSky}$	ε^{Top}_{Lamp}	A_{Lamp}	$\tau_{CovFIR}\tau^{U}_{ThScrFIR}\tau^{U}_{BlScrFIR}$
$R_{LampCov,in}$	ε^{Top}_{Lamp}	A_{Lamp}	$\tau^{U}_{ThScrFIR}\tau^{U}_{BlScrFIR}$
$R_{LampThScr}$	ε^{Top}_{Lamp}	A_{Lamp}	$U_{BlScr}\tau^{U}_{BlScrFIR}$
$R_{LampBlScr}$	ε^{Top}_{Lamp}	A_{Lamp}	U_{BlScr}
$R_{FIR\_LampCan}$	$\varepsilon^{Bottom}_{Lamp}$	A_{Lamp}	$1-e^{-K_{FIR}LAI}$
$R_{LampPipe}$	$\varepsilon^{Bottom}_{Lamp}$	A_{Lamp}	$0.49\pi l_{Pipe}\varphi_{Pipe,e}e^{-K_{FIR}LAI}$
$R_{FIR\_\ LampFlr}$	$\varepsilon^{Bottom}_{Lamp}$	A_{Lamp}	$(1-0.49\pi l_{Pipe}\varphi_{Pipe,e})e^{-K_{FIR}LAI}$
$R_{FIR\_IntLampCan}$	$\varepsilon_{IntLamp}$	$A_{IntLamp}$	1
$R_{GroPipeCan}$	$\varepsilon_{GroPipe}$	$\pi l_{GroPipe}\varphi_{GroPipe,e}$	1
$R_{BlScrSky}$	ε_{BlScr}	1	$\tau_{CovFIR}U_{BlScr}\tau^{U}_{ThScrFIR}$
$R_{BlScrCov,in}$	ε_{BlScr}	1	$U_{BlScr}\tau^{U}_{ThScrFIR}$
$R_{BlScrThScr}$	ε_{BlScr}	1	$U_{BlScr}U_{ThScr}$
$R_{CanBlScr}$	ε_{Can}	$1-e^{-K_{FIR}LAI}$	$\tau_{LampFIR}U_{BlScr}$
$R_{PipeBlScr}$	ε_{Pipe}	$\pi l_{Pipe}\varphi_{Pipe,e}$	$\tau_{LampFIR}U_{BlScr}0.49\pi l_{Pipe}\varphi_{Pipe,e}e^{-K_{FIR}LAI}$
$R_{FlrBlScr}$	ε_{Flr}	1	$\tau_{LampFIR}U_{BlScr}(1-0.49\pi l_{Pipe}\varphi_{Pipe,e})e^{-K_{FIR}LAI}$

for the calculation of $R_{LampSky}$, $R_{LampCov,in}$, $R_{LampThScr}$, $R_{LampBlScr}$, $R_{FIR\_LampCan}$, $R_{LampPipe}$, $R_{FIR\_LampFlr}$, $R_{FIR\_IntLampCan}$, $R_{GroPipeCan}$, $R_{BlScrSky}$, $R_{BlScrCov,in}$, $R_{BlScrThScr}$, $R_{CanBlScr}$, $R_{PipeBlScr}$, and $R_{FlrBlScr}$.

The areas A_i and the view factors $F_{i,j}$ used are given in Table A.1. The top-lights and blackout screen obstruct the view between objects in the greenhouse, and the long wave heat exchange was modified accordingly, with the assumption that the blackout screen is directly below the thermal screen. It was assumed that the canopy fully hides the inter-lights and the grow pipes, so that these two objects only exchange FIR with the canopy. The lamp areas A_{lamp} and $A_{IntLamp}$ are parameters that depend on the choice of the lamps. The emissivity of the top-lights ε_{Lamp} was different between the top and the bottom side of the lamp. Thus, two emissivity values ε_{Lamp}^{Top}, $\varepsilon_{Lamp}^{Bottom}$ were used, depending on the direction of radiation emitted from the lamp.

A.4. Convection and capacities

The convective heat transfers added to the model were calculated as:

$$H_{AirBlScr} = c_{HECblScrAir}(T_{Air} - T_{BlScr})\left(Wm^{-2}\right) \quad (A28)$$

$$H_{LampAir} = c_{HEClampAir}(T_{Lamp} - T_{Air})\left(Wm^{-2}\right) \quad (A29)$$

$$H_{IntLampAir} = c_{HECintLampAir}(T_{IntLamp} - T_{Air})\left(Wm^{-2}\right) \quad (A30)$$

$$H_{GroPipeAir} = c_{HECgroPipeAir}(T_{GroPipe} - T_{Air})\left(Wm^{-2}\right) \quad (A31)$$

where $c_{HECblScrTop}$, $c_{HECblScrAir}$, $c_{HEClampAir}$, $c_{HECintLampAir}$, and $c_{HECgroPipeAir}$ (W m^{-2} K^{-1}) are the heat exchange coefficients between, respectively, the blackout screen and the air in the top compartment; the air in the main compartment and the blackout screen, the top-lights, the inter-lights, and the grow pipes.

The heat exchange coefficients between the blackout screen and the surrounding air was analogous to that of the thermal screen in the Vanthoor model (De Zwart, 1996; Vanthoor and De Visser, et al., 2011):

$$c_{HECblScrAir} = 1.7U_{BlScr}|T_{Air} - T_{BlScr}|^{0.33}.\left(Wm^{-2}\right) \quad (A32)$$

The heat exchange coefficient between the air and the grow pipes was calculated analogously to that of the pipe rail system in the Vanthoor model (De Zwart, 1996; Vanthoor and De Visser, et al., 2011):

$$c_{HECgroPipeAir} = 1.99\pi\varphi_{groPipe,e} l_{GroPipe} \left|T_{GroPipe} - T_{BlScr}\right|^{0.33} . (\mathrm{Wm^{-2}}) \quad \text{(A33)}$$

The energy extracted from the lamps by an active cooling system was assumed to be a fixed fraction of the energy input to the lamps:

$$H_{LampCool} = \eta_{LampCool} Q_{LampIn} . (\mathrm{Wm^{-2}}) \quad \text{(A34)}$$

The heat capacity of the grow pipes was calculated analogously to that of the pipe rail system:

$$cap_{GroPipe} = 0.25\pi l_{GroPipe} \left(\left(\varphi^2_{GroPipe,e} - \varphi^2_{GroPipe,i} \right) \cdot \rho_{Steel} c_{p,Steel} + \varphi^2_{GroPipe,i} \rho_{Water} c_{p,Water} \right) (\mathrm{W\,m^{-2}}) \quad \text{(A35)}$$

A.5. Blackout screen

Blackout screens are often used in illuminated greenhouses to prevent light from the greenhouse to penetrate to the outside and cause light pollution. Depending on local regulations, growers might be required to use blackout screens if the lamps are on for certain hours of the night. In GreenLight, a blackout screen is used in addition to the thermal screen used in the Vanthoor model. The blackout screen is installed directly below the thermal screen, influencing the FIR exchange between the greenhouse objects, as described in section A.3. In addition, the blackout screen influences air flow between the main and top greenhouse compartment. For this, first the air flows through each of the screens is calculated. Air flow through the thermal screen is:

$$f_{ThScr} = U_{ThScr} K_{ThScr} \left|T_{Air} - T_{Top}\right|^{0.66} + \frac{1 - U_{ThScr}}{\rho^{Mean}_{Air}} \left(0.5 \rho^{Mean}_{Air} (1 - U_{ThScr}) g \left|\rho_{Air} - \rho_{Top}\right|\right)^{0.5} (\mathrm{m^3\,m^{-2}\,s^{-1}}) \quad \text{(A36)}$$

and airflow through the blackout screen is:

$$f_{BlScr} = U_{BlScr} K_{BlScr} \left|T_{Air} - T_{Top}\right|^{0.66} + \frac{1 - U_{BlScr}}{\rho^{Mean}_{Air}} \left(0.5 \rho^{Mean}_{Air} (1 - U_{BlScr}) g \left|\rho_{Air} - \rho_{Top}\right|\right)^{0.5} (\mathrm{m^3\,m^{-2}\,s^{-1}}) \quad \text{(A37)}$$

here, U_{ThScr} and U_{BlScr} are the closure of the thermal and blackout screens, respectively (0 representing an open screen and 1 a fully closed screen); K_{ThScr} and K_{BlScr} ($\mathrm{m^3\,m^{-2}\,K^{-0.66}\,s^{-1}}$) are the screen flux coefficients of the thermal and blackout screens; g ($\mathrm{m\,s^{-2}}$) is gravitational acceleration; ρ_{Air} ($\mathrm{kg\,m^{-3}}$) is the density of air in the main compartment; ρ_{Top} ($\mathrm{kg\,m^{-3}}$) is the density of air in the top compartment; and ρ^{Mean}_{Air} ($\mathrm{kg\,m^{-3}}$) is the average of ρ_{Air} and ρ_{Top}.

It should be noted that in Vanthoor and Stanghellini, et al. (2011), the outside air is used in the above equation instead of the air in the top compartment. However, GreenLight follows here the equations of De Zwart (1996) where the air in the top compartment is used.

Once the air flow through each screen is calculated, it is assumed that the final rate of air flow through the screens layer is the minimum between the two air flows:

$$f_{scr} = \min\left\{f_{ThScr}, f_{BlScr}\right\} (\mathrm{m^3\,m^{-2}\,s^{-1}}) \quad \text{(A38)}$$

where f_{Scr} is the airflow between the main and top greenhouse compartments.

Condensation of water vapour in the main compartment onto the blackout screen was defined as:

$$MV_{AirBlScr} = \max\left\{0,\ 6.4 \times 10^{-9} c_{HECblScrAir} \left(VP_{Air} - VP_{BlScr}\right)\right\} \quad (\mathrm{kg\,m^{-2}\,s^{-1}}) \quad \text{(A39)}$$

where $c_{HECblScrAir}$ ($\mathrm{W\,m^{-2}\,K^{-1}}$) is the heat exchange coefficient between the air and the blackout screen, defined above; VP_{Air} (Pa) is the vapour pressure of the air in the main compartment; and VP_{BlScr} is the saturated vapour pressure at the temperature of the blackout screen T_{BlScr}.

The condensation on the blackout screen reduced the vapour concentration of the air in the main compartment (expression not in bold remained the same as in the Vanthoor model):

$$cap_{VP_{Air}} \dot{VP}_{Air} = MV_{CanAir} - MV_{AirThScr} - MV_{AirTop} - MV_{AirOut} - \boldsymbol{MV_{AirBlScr}} (\mathrm{kg\,m^{-2}\,s^{-1}}) \quad \text{(A40)}$$

Furthermore, the condensation transferred latent heat from the air to the blackout screen:

$$L_{AirBlScr} = \Delta H \cdot MV_{AirBlScr} (\mathrm{W\,m^{-2}}) \quad \text{(A41)}$$

where ΔH ($\mathrm{J\,kg^{-1}}$) is the latent heat of evaporation of water.

The parameters used for the blackout screen are given in Table A.2. It was assumed that the blackout screen behaves similarly to a thermal screen, with the exception that 99% of the light is blocked by the blackout screen, and that the blackout screen does not contain aluminium strips, and thus has a higher emissivity than the thermal screen.

Table A2 – GreenLight parameters used for the blackout screen in the current study.

Notation	Meaning	Unit	Value
$\epsilon_{BlScrFIR}$	FIR emission coefficient of the blackout screen	–	0.67
ρ_{BlScr}	Density of the blackout screen	$\mathrm{kg\,m^{-3}}$	0.2×10^3
$\rho_{blScrNIR}$	NIR reflection coefficient of the blackout screen	–	0.35
$\rho_{blScrPAR}$	PAR reflection coefficient of the blackout screen	–	0.35
$\tau_{blScrNIR}$	NIR transmission coefficient of the blackout screen	–	0.01
$\tau_{blScrPAR}$	PAR transmission coefficient of the blackout screen	–	0.01
$\tau_{blScrFIR}$	FIR transmission coefficient of the blackout screen	–	0.7
$c_{p,BlScr}$	Specific heat capacity of the blackout screen	$\mathrm{J\,kg^{-1}\,K^{-1}}$	1.8×10^3
h_{BlScr}	Thickness of the blackout screen	m	0.35×10^{-3}
K_{BlScr}	Blackout screen flux coefficient	$\mathrm{m^3\,m^{-2}\,K^{-0.66}\,s^{-1}}$	5×10^{-4}

A.6. Leakage ventilation

In the Vanthoor model, it is assumed that the leakage ventilation is equally distributed between the main and top compartment: half the leakage ventilation comes from the top compartment and half comes from the main compartment:

$$f_{VentRoof} = \eta_{InsScr} f''_{VentRoof} + c_{LeakTop} f_{leakage} \left(m^3\ m^{-2}\ s^{-1}\right) \quad (A42)$$

$$f_{VentSide} = \eta_{InsScr} f''_{VentSide} + (1 - c_{LeakTop}) f_{leakage} \left(m^3\ m^{-2}\ s^{-1}\right) \quad (A43)$$

maintenance respiration of the fruits. $MC_{FruitHar}$ (mg m^{-2} s^{-1}) is the rate of fruit harvest, and it is performed in a similar fashion to leaf pruning:

$$MC_{FruitHar} = \max\{0,\ C_{Fruit} - C^{Max}_{Fruit}\} \quad \left(mg\ m^{-2}\ s^{-1}\right) \quad (A45)$$

where C^{Max}_{Fruit} is the maximum amount of fruit allowed to be on the crop before harvest is performed. In other words, harvest is only done once C_{Fruit} reaches C^{Max}_{Fruit}. When that happens, harvest is performed to reduce C_{Fruit} back to C^{Max}_{Fruit}.

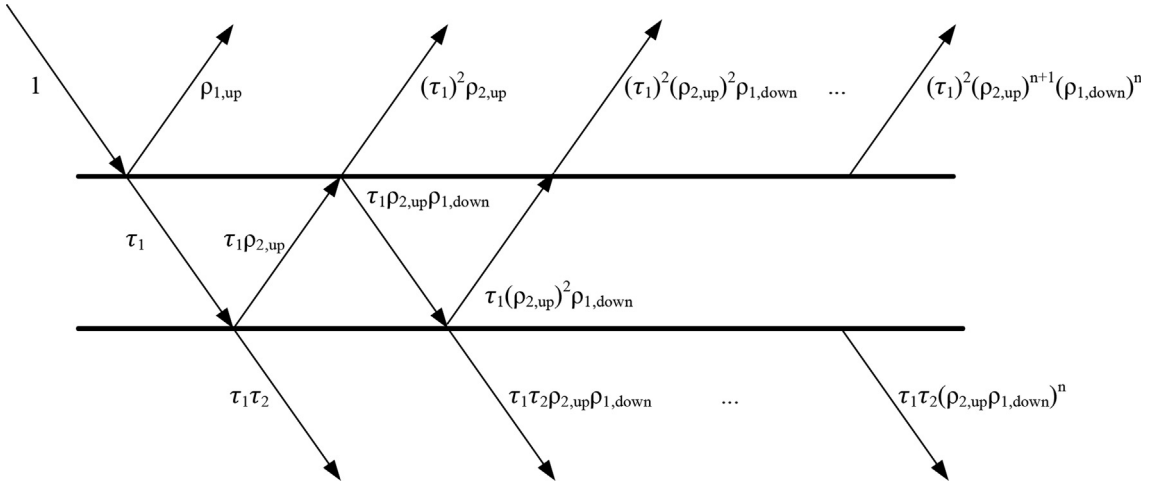

Fig. A1 – Trajectory of radiation coming from above and passing through a double layer. Values near the arrow represent fractions of the original incoming radiation. The reflectivity of the double layer is an infinite sum of the values of the arrows pointing up at the top of the figure, while the transmissivity of the double layer is an infinite sum of the arrows pointing down at the bottom of the figure.

where $c_{LeakTop}$ (–) is assumed to be 0.5. In GreenLight, this value may be adjusted. Indeed, for the trial described in this study, where compartments within a greenhouse were considered and not a standalone greenhouse, it was assumed that the majority of the leakage ventilation comes from the top of the greenhouse, with $c_{LeakTop}$ set at 0.9.

A.7. Crop model

The focus of GreenLight is greenhouse energy use and indoor climate. To simplify the simulations, only the total amount of dry mass in the fruit was considered, but not the various fruit development stages. While this may influence the timing of fruit harvest compared to the Vanthoor model, the total harvest would not be affected. The result is that while in the Vanthoor model there are 50 stages of fruit development, in GreenLight there is only one fruit development stage n_{Dev}, and the number of fruits is not considered. Harvest is performed when the total fruit dry weight reaches a certain threshold. The resulting equation is thus:

$$\dot{C}_{Fruit} = MC_{BufFruit} - MC_{FruitAir} - MC_{FruitHar} \left(mg\ m^{-2}\ s^{-1}\right) \quad (A44)$$

where $MC_{BufFruit}$ (mg m^{-2} s^{-1}) is dry matter flow from the carbohydrates buffer to the fruits and $MC_{FruitAir}$ (mg m^{-2} s^{-1}) is the

REFERENCES

Ahamed, M. S., Guo, H., & Tanino, K. (2018). A quasi-steady state model for predicting the heating requirements of conventional greenhouses in cold regions. *Information Processing in Agriculture*, 5, 33–46. https://doi.org/10.1016/j.inpa.2017.12.003.

Ahamed, M. S., Guo, H., & Tanino, K. (2019). Energy saving techniques for reducing the heating cost of conventional greenhouses. *Biosystems Engineering*, 178, 9–33. https://doi.org/10.1016/j.biosystemseng.2018.10.017.

Altes-Buch, Q., Quoilin, S., & Lemort, V. (2019). Greenhouses: A Modelica library for the simulation of greenhouse climate and energy systems. In *Proceedings of the 13th International Modelica Conference, Regensburg, Germany, March 4–6, 2019* (Vol. 157, pp. 533–542). https://doi.org/10.3384/ecp19157533.

Both, A.-J., Bugbee, B., Kubota, C., Lopez, R. G., Mitchell, C., Runkle, E. S., et al. (2017). Proposed product label for electric lamps used in the plant Sciences. *HortTechnology*, 27(4), 544–549. https://doi.org/10.21273/horttech03648-16.

Bugbee, B. (2017). Economics of LED lighting. In S. Dutta Gupta (Ed.), *Light emitting diodes for agriculture* (pp. 81–99). Singapore: Springer Nature Singapore. https://doi.org/10.1007/978-981-10-5807-3.

De Zwart, H. F. (1996). Analyzing energy-saving options in greenhouse cultivation using a simulation model. *Landbouwuniversiteit Wageningen*, 1–236.

De Zwart, H. F., Baeza, E., Van Breugel, B., Mohammadkhani, V., & Janssen, H. (2017). *De uitstralingmonitor*.

Dieleman, A., Janse, J., De Gelder, A., Kempkes, F., De Visser, P., Lagas, P., et al. (2015). *Tomaten belichten met minder elektriciteit*. Bleiswijk.

Dueck, T., Janse, J., Eveleens, B. A., Kempkes, F. L. K., & Marcelis, L. (2012). Growth of tomatoes under hybrid LED and HPS lighting. *Acta Horticulturae, 1*(952), 335–342. https://doi.org/10.17660/ActaHortic.2012.952.42.

Dueck, T., Janse, J., Schapendonk, A. H. C. M., Kempkes, F., Eveleens, B., Scheffers, K., et al. (2010). *Lichtbenuttig van tomaat onder LED en SON-T belichting*. Wageningen.

Dutta Gupta, S. (2017). In D. Gupta (Ed.), *Light emitting diodes for agriculture*. Singapore: Springer Nature. https://doi.org/10.1007/978-981-10-5807-3.

Golzar, F., Heeren, N., Hellweg, S., & Roshandel, R. (2018). A novel integrated framework to evaluate greenhouse energy demand and crop yield production. *Renewable and Sustainable Energy Reviews, 96*, 487–501. https://doi.org/10.1016/j.rser.2018.06.046 (June).

Hemming, S., Balendonck, J., Dieleman, J. A., De Gelder, A., Kempkes, F. L. K., Swinkels, G. L. A. M., et al. (2017). Innovations in greenhouse systems - energy conservation by system design, sensors and decision support systems. *Acta Horticulturae, 1170*, 1–15. https://doi.org/10.17660/ActaHortic.2017.1170.1.

Heuvelink, E., Li, T., & Dorais, M. (2018). Crop growth and yield. In E. Heuvelink (Ed.), *Tomatoes* (2nd ed., pp. 89–135). Wallingford: Cabi.

Holst, N. (2013). A universal simulator for ecological models. *Ecological Informatics, 13*, 70–76. https://doi.org/10.1016/J.ECOINF.2012.11.001.

Holst, N. (2019). *Universal simulator 2.1.18a*. Retrieved April 3, 2019, from www.ecolmod.org.

The DesignLights Consortium. (2020). *Horticultural lighting qualified products list*. https://www.designlights.org/horticultural-lighting/. (Accessed 30 March 2020).

Jamieson, P. D., Porter, J. R., & Wilson, D. R. (1991). A test of the computer simulation model ARCWHEAT1 on wheat crops grown in New Zealand. *Field Crops Research, 27*(4), 337–350. https://doi.org/10.1016/0378-4290(91)90040-3.

Katzin, D. (2020). *DyMoMa - dynamic modelling for MATLAB*. https://doi.org/10.5281/zenodo.3697908. github.com/davkat1/GreenLight.

Kim, H. J., Lin, M. Y., & Mitchell, C. A. (2019). Light spectral and thermal properties govern biomass allocation in tomato through morphological and physiological changes. *Environmental and Experimental Botany, 157*, 228–240. https://doi.org/10.1016/j.envexpbot.2018.10.019.

Körner, O., & Holst, N. (2017). An open-source greenhouse modelling platform. *Acta Horticulturae, 1154*, 241–248. https://doi.org/10.17660/ActaHortic.2017.1154.32.

Lopez-Cruz, I. L., Fitz-Rodríguez, E., Salazar-Moreno, R., Rojano-Aguilar, A., & Kacira, M. (2018). Development and analysis of dynamical mathematical models of greenhouse climate : A review. *European Journal of Horticultural Science, 83*(5), 269–280. https://doi.org/10.17660/eJHS.2018/83.5.1.

Marcelis, L., Buwalda, F., Dieleman, A., Dueck, T., Elings, A., De Gelder, A., et al. (2014). Innovations in crop production: A matter of physiology and technology. *Acta Horticulturae, 1037*, 39–46. https://doi.org/10.17660/ActaHortic.2014.1037.1.

Marcelis, L., Costa, J. M., & Heuvelink, E. (2019). Achieving sustainable greenhouse production: Present status, recent advances and future developments. In *Achieving sustainable greenhouse production* (pp. 1–12).

Marcelis, L., & Heuvelink, E. (Eds.). (2019). *Achieving sustainable greenhouse cultivation* (1st ed.). London: Burleigh Dodds Science Publishing. https://doi.org/10.1201/9780429266744.

Mitchell, C. A., Dzakovich, M. P., Gomez, C., Burr, J. F., Hernández, R., Kubota, C., et al. (2015). Light-emitting diodes in horticulture. *Horticultural Reviews, 43*, 1–87. https://doi.org/10.1002/9781119107781.ch01.

Nelson, J. A., & Bugbee, B. (2014). Economic analysis of greenhouse lighting: Light emitting diodes vs. High intensity discharge fixtures. *PloS One, 9*(6), e99010. https://doi.org/10.1371/journal.pone.0099010.

Nelson, J. A., & Bugbee, B. (2015). Analysis of environmental effects on leaf temperature under sunlight, high pressure sodium and light emitting diodes. *PloS One, 10*(10), e0138930. https://doi.org/10.1371/journal.pone.0138930.

Ouzounis, T., Giday, H., Kjaer, K. H., & Ottosen, C. O. (2018). LED or HPS in ornamentals? A case study in roses and campanulas. *European Journal of Horticultural Science, 83*(3), 1611–4434. https://doi.org/10.17660/eJHS.2018/83.3.6.

Ouzounis, T., Rosenqvist, E., & Ottosen, C. O. (2015). Spectral effects of artificial light on plant physiology and secondary metabolism: A review. *HortScience, 50*(8), 1128–1135. https://doi.org/10.21273/HORTSCI.50.8.1128.

Pattison, P. M., Hansen, M., & Tsao, J. Y. (2018). LED lighting efficacy: Status and directions. *Comptes Rendus Physique, 19*(3), 134–145. https://doi.org/10.1016/j.crhy.2017.10.013.

Stanghellini, C., van't Ooster, B., & Heuvelink, E. (2019). *Greenhouse horticulture: Technology for optimal crop production* (1st ed.). Wageningen: Wageningen Academic Publishers.

Van Beveren, P. J. M., Bontsema, J., Van Straten, G., & Van Henten, E. J. (2015b). Optimal control of greenhouse climate using minimal energy and grower defined bounds. *Applied Energy, 159*, 509–519. https://doi.org/10.1016/j.apenergy.2015.09.012.

Van Beveren, P. J. M., Bontsema, J., Van Straten, G., & Van Henten, E. J. (2015a). Minimal heating and cooling in a modern rose greenhouse. *Applied Energy, 137*, 97–109. https://doi.org/10.1016/j.apenergy.2014.09.083.

Vanthoor, B., De Visser, P. H. B., Stanghellini, C., & Van Henten, E. J. (2011). A methodology for model-based greenhouse design: Part 2, description and validation of a tomato yield model. *Biosystems Engineering, 110*(4), 378–395. https://doi.org/10.1016/j.biosystemseng.2011.08.005.

Vanthoor, B., Stanghellini, C., van Henten, E. J., & de Visser, P. H. B. (2011). A methodology for model-based greenhouse design: Part 1, a greenhouse climate model for a broad range of designs and climates. *Biosystems Engineering, 110*(4), 363–377. https://doi.org/10.1016/j.biosystemseng.2011.06.001.

Viršilė, A., Olle, M., & Duchovskis, P. (2017). LED lighting in horticulture. In S. Dutta Gupta (Ed.), *Light emitting diodes for agriculture* (pp. 113–147). Singapore: Springer Nature Singapore.